SDC-92-321

SDC
SOLENOIDAL DETECTOR NOTES

SDC 9-CM MUON DRIFT TUBE: ELECTROMECHANICAL STUDIES-I

September 3, 1992

G. Yasuda and R.H. Milburn
Tufts University

September 3, 1992

SDC 9-CM MUON DRIFT TUBE : Electromechanical Studies – I

G. Yasuda and R. H. Milburn
Tufts University
Medford, MA 02155

ABSTRACT

We present a collection of studies relating to the measurement precision of the 9cm diameter field-shaping drift chamber cells being developed for use in the SDC muon system. This precision depends not only upon the gas and the electrostatic field configuration but also upon the sense wire location, which in turn depends upon the wire tension and on the interplay of gravitational and electrostatic forces. A precise control of these factors during detector cell manufacture and knowledge of them during detector operation is imperative. In the following sections we investigate a loosely correlated variety of these problems including electrostatic simulations of the drift-time and isochrone dependencies upon sense wire positions, and predictions of the electrostatic effects on equilibrium wire configuration, stability and mechanical vibrational spectrum. We also include an electrostatic simulation showing the effects, on field and drift-timing, of the plastic supports to the metal field-shaping electrodes. This report is necessarily preliminary insofar as the drift cell configuration and operating conditions are still under development. It is hoped that the following discussion and illustrations will facilitate this development process by providing a theoretical underpinning to laboratory observations and their interpretation in shop and field. It is also hoped that they may inspire some invention of practical quality control systems such as might be based upon measurement of the mechanical wire vibration frequencies.

1. Introduction

We report here on a collection of studies relevant to the design, manufacture and operation of the $9cm$ diameter drift chamber modules being developed for the SDC muon system – in particular for the "barrel" system in which typical modules contain sense wires as long as $9meters$ which are supported only at the ends. These wires will inevitably sag under gravity $1-2mm$ $(1,000-2,000\mu m)$ at their centers and the displacement will be further influenced – favorably and/or unfavorably – by the presence of electrostatic forces. This displacement of a wire relative to the

remaining electrodes will affect the drifting times of electrons from a passing ionizing track and thus also the precision of track location inferred from this timing. Bending of the external module tube will have an additional effect. The success of an assembly of these muon detector drift modules in providing a collective precision of the order of $100 - 200\mu m$ for the measurement of fast muon momenta, and for triggering on them, requires a correspondingly precise understanding of the "figure" of the individual wires throughout the detector, under operating conditions. By implication, this further demands that adequate quality assurance procedures be provided, especially with regard to determining the *wire tensions*, from the time the modules are assembled through their installation in the detector – and if practicable, beyond.

2. Electrostatic Simulation

The CERN Library program "POISSON" was used for the basic electrostatic potential calculations. This system uses a finite-element solution of the Laplace Equation and, although developed primarily for magnet calculations, it also handles electrostatic boundary conditions at dielectrics very nicely. The graphical display portion of "POISSON" was modified to calculate and illustrate the electric field lines and the electron drift times along them, using a set of internal tables for the drift velocity dependence on electric field for various gases of interest. It also generates HBOOK NTUPLES characterizing the timing of electrons drifting from a passing ionizing track. The PAW analysis of these will be illustrated in some of the following figures. A more detailed description of these calculations is given in Appendix I.

An additional program was written, called "WIRECAP", again utilizing POISSON field calculations, to calculate the Maxwell Stress Tensor in the vicinity of the sense wire and thus to establish the electrostatic force on the wire. It also determined the wire potential itself by integrating the electric field around the wire and applying Gauss' Law. At this point, it should be noted that the POISSON system is based upon a finite element solution of the Laplace Equation for a set of regions whose perimeters can be fitted by a warped but finite triangular mesh, and for appropriate conditions on these boundaries. In consequence, POISSON does very well with complex boundaries composed of lines of finite length, but very poorly at field calculations near singularities such as represented by sense wires.

As the result of this we were required to approximate the quasi-singular sense wire by a small ($2mm$ radius) circle held at the appropriate potential. The choice of this potential was established iteratively by using the above WIRECAP program to determine the wire potential, and then making corrections to the POISSON input and rerunning it. The assumption of a constant potential at $2mm$ radius is an approximation, but we find no evidence that it has a significant influence on the precision of the field distribution over the bulk of the drifting region.

In this connection it is appropriate to note here that our POISSON-based system is in several ways complementary to the CERN drift-chamber analysis sys-

tem called "GARFIELD" (cf. CERN Library: POOL-W5050) whose calculations are based upon superposition of the fields of a collection of line singularities – actually of cylinders of very small diameter – including one or more "sense wires." In GARFIELD a conducting surface boundary is represented by a suitably dense array of nearby wires held at the same potential. GARFIELD thus represents very well the field near a sense wire, and this feature allows it to calculate quite credibly the electron amplification and ion drift characteristics, and finally the expected electronic signal shape. On the other hand, dielectric interfaces are not easily coped with. For the intermediate region, GARFIELD and our POISSON-based systems should be essentially equivalent. For present purposes we prefer the latter system because its interface to PAW facilitates subsequent analyses of timing etc., because it handles the field-shaping electrodes and dielectrics correctly, and finally because (we think) its output graphics give a more accurate and esthetic depiction of the field behavior at the various boundaries.

3. Linearity and Wire Displacement Effects

The presently accepted muon drift cell design, as developed at the Univ. of Washington, is circular with a central sense wire and two adjacent planar electrodes to shape the field and provide a relatively linear drifting field in the vicinity of the median plane. These field-shaping electrodes are supported by a dielectric material, "Noryl", with a dielectric constant $\epsilon = 2.8$, on either side of the sense wire and they need not be at the same potential as the wire. The electrode widths, locations and voltages are designed to provide quasi-uniform drift regions extending $\pm 4.5cm$ in each direction from the wire. The $4.5cm$ dimension is a limit required to keep the maximum drift time under $1\mu s$ (governed by data pipe-line limitations, etc.) while using a non-flammable and inexpensive gas such as the $Ar - CO_2$ mixture now under consideration. This choice is itself governed by perceptions of prudence, reliability and cost in respect to the very large scale and potential leakage surface area of the ultimate detector assembly.

The spatial precision attainable using these proposed drift chamber modules depends upon several distinct factors:

- (1) the precision of mechanical location of the two ends of the sense wire where they pass through crimp tubes as much as $9m$ apart;
- (2) a knowledge of the wire configuration between its ends, as governed by gravitational and electrostatic stresses and by the wire tension; and
- (3) the uncertainty in the positions of the field shaping electrodes and of the outer drift tube wall with respect to the central wire following tube assembly into larger modules and as strained in their ultimate mounting on the SDC detector.

Pending detailed laboratory studies of actual drift tube performance in the presence of manufacturing idiosyncracies and environmental fluctuations, and as a guide to making such studies, a theoretical investigation of factors (2) and (3) was mounted early in 1992, based on electrostatic modelling. Initially, for the sake of concreteness and in the face of a changing spectrum of parameters, a prototype SDC mechanical design was used and a 75 μm diameter sense wire was assumed. We further assumed the gas to be Ar:CO_2 (90:10). The wire and the electrodes are assumed to be at various typical potentials, as suggested by knowledgeable colleagues. Wire potentials 6500 V down to 4500 V are used, with field electrodes at potentials ranging from the wire potential downward. Further variations will no doubt be required in the future and can be incorporated easily. However, a number of observations emerge which are largely independent of these details and these are sufficiently instructive to justify this initial report. Now, some results:

4.. Isochrones & Drift Lines vs Operating Potentials : 75μm wire

These results are most compactly presented in a sequence of heavily annotated figures, all pertaining to a 75 μm diameter sense wire and 9cm diameter drift tube filled with with Ar-CO_2 (90-10) at 1 atmosphere. (A parallel presentation of similar results for a 90μm diameter wire commences in Section 9., following.) These may be summarized as follows:

FIGURE 1

The basic model drift tube in cross section with both sense wire and field-shaping electrodes at 6500V, showing equipotentials (solid lines), electric field lines (dotted) and isochrones (*** every 50 nsec, ooo every 250 nsec). SI units are used throughout with dimensions in meters, etc, except as specifically noted.

Note: Since 1$nsec$ $\simeq$ 50μm or so, it is obvious from the curvature of the isochrones that at most only a few millimeters of ionizing track will contribute to the leading edge of a signal discriminating a 100μm position resolution.

FIGURE 2

Same as in Figure 1 but with anode and the field shaping electrodes at 5500V. The distributions of equipotentials and of electric field lines are identical to those in Figure 1 (from the homogeneity of the Laplace Equation) but the isochrones are different because the "operating point" in the drift-velocity vs field curve is different. This is shown in the following two figures.

FIGURE 3

A plot of drift velocity vs electric field for all the points plotted in Figure 1 ($6500V$). These points also sketch out the input data used (for better or for worse!) to represent the gas in question. The accumulation of points around $110,000V/m$ ($1100V/cm$) represents the field and drift velocity affecting the bulk of the trajectories reaching the ends of the drift region in Figure 1.

FIGURE 4

A plot of drift velocity vs field for all the points plotted in Figure 2. The difference between Figures 3 and 4 is that the latter is operated at $5500V$ (both the electrode and the wire).The accumulation of points for this is around $95,000V/m$ ($950V/cm$).

It is seen that by varying the drift field gradient and/or the characteristics of the gas mixture one has the possibility of "tuning" the tube performance in the sense of adjusting the linearity of the position-vs-time dependence and the curvature of the isochrones (which affects the output pulse height and shape). Qualititatively, the more negative the slope of the velocity dependence on field, the larger will be the radii of curvature of the isochrones, and the larger will be the number of electrons from an ionizing track that arrive at the sense wire within a resolution time.

5. Linearity of Position vs Drift Time : 75 μm wire

While the primary requirement for a drift cell is to have a monotonic relationship between measured drift time and the incident track position, the more linear this relation is the simpler the programming required to translate integer TDC data into track coordinates. To the extent that this translation must be effected in real time, as with a low-level hardware trigger processor, the more linear this relationship the better.

FIGURE 5

Linearity of the $6500V$ tube in Figure 1 The integrated drift times from a particular point, X, along the three trajectories near the tube midline (cf. Figure 1.) are fitted to a linear function of X with a "mean" drift velocity. These are the trajectories which will contribute to the leading edge of the resultant timing signal. More specifically, in Figure 5, the discrepancies from linearity, multiplied by the drift velocity at the points in question, are plotted versus X. This is achieved, within the PAW analysis system, by plotting the function

$$TIMER3(X) = TIME + 0.98523 - 21.804(X)$$

of drift $TIME$ from position X, versus X. The result shows that linearity to within $160\mu m$ holds over the region from $2cm$ away from the wire (which is located at

$X = 0.045m$) out to the wall at $9.0cm$. The mean drift velocity is $1/21.804 = 4.743cm/\mu s$. The offset in the abscissa has been set arbitrarily to $0cm$. Note, also, that the three trajectories shown correspond to about $3mm$ of ionizing particle track.

FIGURE 6

Same as Figure 5 except for a voltage of $5500V$ on the electrodes and the wire. Here , the results show that linearity has been improved to within $80\mu m$. The fitted function is now

$$TIMER4(X) = TIME + 0.94129 - 20.938(X)$$

corresponding to a mean drift velocity of $4.776cm/\mu s$.

6. Timing & Position Effects of Wire Displacement : 75 μm wire

A series of calculations were made, for various potential distributions, gases, etc., with the $2mm$ circle representing the sense wire displaced by small increments $(1 - 2mm)$ from its normal central position. In practical operation, these can come about from wire sag under gravity and electric forces, or equivalently from the bending of the outer tube assembly relative to an otherwise straight sense wire, or both. The most evident effects on the drift tube's measurement capability are illustrated by repeating the linearity tests of Section 5 while using the same fitting functions as for the undisplaced wire.

FIGURE 7

This figure shows the effect of displacing the anode wire $2mm$ "up" (in Figure 1), that is, perpendicular to the drift direction. This is the case with $6500V$ on both the $75\mu m$ wire and field-shaping electrodes.

FIGURE 8

The same as in Figure 7 but with the wire displaced $2mm$ " downwards."

In both of these cases, the effects on timing of $2mm$ displacements perpendicular to the drift direction are seen to be negligible.

FIGURE 9

Here the $2mm$ wire displacement is towards the "left" (- X, in Figure 1) and is antiparallel to the drift direction, thus elongating the drift region in the right-hand half of the tube.

FIGURE 10

The same as in Figure 9 but with the $2mm$ wire displacement to the "right" (+ X, in Figure 1), thus shortening the drift region on the right.

Figures 9 and 10 may be compared with Figure 1 to verify that, while the linearity is only slightly effected, there is a displacement in the inferred track position of about $\pm 1.6mm$, or 20% *less* than the $2mm$ one might expect from the wire motion alone. This discrepancy is $\approx 400\mu m$, for a $2mm$ wire displacement. It implies that an unsuspected mispositioning of the tube wall by $1mm$ along the drift direction will introduce a corresponding $200\mu m$ systematic error in the inferred track position relative to a wire whose position is otherwise known. This has obvious implications for the control of the body positions of the drift tubes, and not only their ends, as they are mounted in larger assemblies.

This annoying effect depends upon the shape of the drift-velocity vs field curve and on the previously described "operating point" along this curve. Comparing the plots of drift velocity versus field for $6500V$ and $5500V$ of applied voltage (Figure 3 and Figure 4 respectively), we can clearly see that with higher fields the "operating region" corresponds to smaller drift velocities, so that the wire displacements affect primarily the slower-drifting electrons. Thus "tuning" the operating point to reduce this wall-displacement effect would appear to increase the isochrone curvature and so reduce the number of initially arriving electrons, and vice versa – perhaps an unfortunate conflict.

7. Electrostatic Stresses: $75\mu m$ wire, 6500V

The wire displacements illustrated in the Figures 7-10 included up and down as well as left and right displacements of $2mm$. For each case the Maxwell Stress Tensor was calculated from the POISSON-fitted electric field components, as described in Section 2, and its surface integral around the sense wire was evaluated by summing over field determinations every 3 degrees in azimuth. This was done for circles of radii $2.2mm$, $2.5mm$, $3.0mm$ and $3.5mm$, since it was evident that for the smaller radii the finite mesh of the POISSON field solution was giving inconsistent results. The $3.0mm$ and $3.5mm$ results were close enough to be identical that they could be taken as meaningful. These model "measurements" can be summarized in terms of effective "anti-spring constants" (force/unit-length of sense wire/unit displacement):

$$k_E\ (up/down) = -1.1\ dyne/cm^2\ ,$$
$$k_E\ (left/right) = 1.5\ dyne/cm^2\ .$$

A negative k_E corresponds to a tendency to stabilize the wire at zero displacement ; a positive k_E to destabilize it. For comparison, the weight per unit length of a $75\mu m$ diameter tungsten wire is

$$f_G = 0.8528\ dyne/cm.$$

Thus, a $2mm$ left or right displacement of the sense wire from center produces a net electrostatic force $(1.5 \times 0.2)/0.8528 = 35\%$ that of the wire's weight alone. The

up/down effect is only 26% that of gravity. It would appear that were gravitational sags of $2mm$ to be considered tolerable, the lateral electrostatic effects would also have to be included.

These "spring constants" k_E are, of course, only first approximations to the actual dependence of the electrostatic force upon wire displacement from its position of symmetry along the tube axis. However, comparison of $\pm 1mm$ and $\pm 2mm$ displacements for the typical electrode and potential distributions here studied have shown us that the next (3rd order) terms are small enough to be neglected for our present purposes insofar as we limit ourselves to displacements less than a few mm. These linear coefficients also facilitate a "theoretical" analysis of the taut-wire problem which can provide some useful insight into the combination of gravitational and electrostatic forces, and the requirements on regulation of the wire tension. [This "theory" will be discussed in more analytical detail in an accompanying report.]

For our immediate purposes we assert that to compute the wire displacement, we need to solve the differential equation (from Newton's Second Law):

$$T_F \frac{d^2y}{dz^2} \pm |k_E| y - \rho\, A\, g = 0 \ , \tag{1}$$

where T_F is the tension, k_E is the magnitude of electrostatic spring constant which can be either positive or negative, y is the displacement perpendicular to the wire, ρ is the density of the wire, A is the cross-sectional area of the wire and g is the component of the acceleration due to gravity in the (-Y) direction (see figure on the following page). Equation (1) can be solved exactly for a wire of length L to give a total maximum (central) displacement for a positive k_E

$$y_{max} = -(f_G/k_E)\ [\sec(\pi L/b) - 1] \ , \tag{2}$$

where $(2\pi/b) = \sqrt{k_E/T_F}$, and $f_G = \rho\ A\ g$. Eq.(2) blows up when L is half a "wavelength" b and $k_E > 0$. For a negative k_E, the maximum displacement is

$$y_{max} = (f_G/k_E)[sech(\lambda L/2) - 1] \ , \tag{3}$$

where $\lambda = \sqrt{|k_E|/T_F}$. In the limit of no electric force, Eqs. (2) and (3) yield the familiar result

$$y_{max} = -\frac{f_G}{8T_F}\ L^2 \ . \tag{4}$$

For the $75\mu m$ diameter wire in question, $500gm$ of tension corresponds to about half the yield strength and gives equivalent "wavelengths" of about $b = 36.4m$ for the left/right cases. Thus unsupported wires of the full $9m$ length are reasonably stable with respect to the run-away of the secant function at $18.2m$.

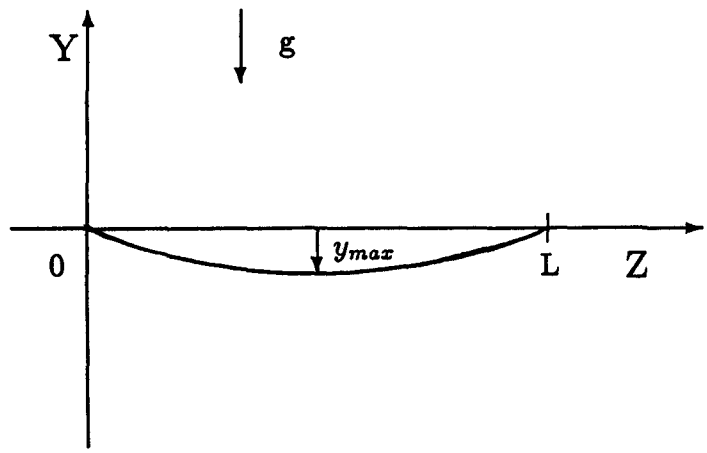

In a practical design with $9m$ unsupported lengths, the basic central gravitational sag is about $1.7mm$ according to Eq. (4) and the electrostatic perturbation adds to it about $0.6mm$ in the worst (left/right) case, totalling $2.3mm$ according to Eq. (2). This is an additional $600\mu m$, so it is evident that in a system based upon such $\sim 9m$ unsupported wire segments the prediction of the precise position of the wire at any point must involve a careful accounting for the electrostatic forces in addition to an understanding of the tension.

The latter, of course, depends on the relationship between the thermal expansion coefficients of the wire and the external tube, and upon the effective Young's Modulus, Y_E, at the tension in question. Using the equation

$$\frac{dF}{dT} = (\alpha_{Al} - \alpha_W)(Y_E A)_W \tag{5}$$

with the coefficients $\alpha_W = 4.5 \times 10^{-6}/°C$ and $\alpha_{Al} = 24 \times 10^{-6}/°C$ for tungsten and aluminum respectively, and with elasticity measurements on $50\mu m$ tungsten wires performed some years ago by W. Oliver for Soudan-2 proportional tubes (Figure 11), we infer that at $20°C$, a temperature excursion of ± 10 $°C$ will produce a $\pm 31.6gm$ variation in wire tension.

In the worst case (when ΔT=-10°C) this can cause an additional $100\mu m$ in gravitational sag in the absence of electrostatic contributions, totalling $1.8mm$. In the presence of a field when the drift tube is operating the total worst-case central sag increases by an additional $100\mu m$ (see figure on the following page).

From earlier analysis in Section 6., we found that by shifting the wire by $2mm$, the inferred track position is shifted by about 80 % of the actual wire displacement. Thus for a temperature change of $-10°C$, the extra sag is about $200\mu m$, which implies that the actual inferred track position is changed by $160\mu m$.

8. Dielectric Field-shaping Electrode Holder

In this section we digress somewhat to examine the effects of the dielectric frame which supports the field shaping electrodes. As above, these POISSON simulations used a $9cm$ diameter drift tube with a $75\mu m$ diameter sense wire at the center, and the same two field electrodes as in Figure 1. Both electrodes and sense wire were at $6500V$.

The flat metal electrodes have a $0.4mm$ thickness and are supported as shown in Figure 1 by a plastic sheath made of the material "Noryl," reputed to have a dielectric constant $\epsilon = 2.8$. The transverse dimension of the Noryl, measured across the field electrodes, is $3.4cm$ and its thickness is here assumed to be $1.4mm$.

The electrostatic simulation was carried out as before with the difference that we analyzed only a single quadrant of the drift tube. (The tube has reflectional symmetry in both drift and transverse directions so that with a centrally-located sense wire we were able to use a finer mesh and thus improve the resolution within the small field-shaping structures.)

Figures 12 – 18 show the resulting plots of equipotential lines for the above plastic electrode shape but with a sequence of dielectric constants: 0.05, 0.2, 1.0 (vacuum), 2.8 (Noryl), 5.0, 20.0 and 40.0 (a quasi-conductor!). These plots show only the dielectric and field-shaping electrode region as we are here interested only in that region. The use of dielectric constants less than 1.0 (corresponding to a negative dielectric susceptibility) qualitatively models the effect one would expect were negative ions to accumulate on the insulating surface and partially cancel the fields generated by positive charges on the metallic field-shaping strip. (In principle, one might in each case determine from the equipotentials the electric field distribution within the slightly conductive Noryl dielectric, and along its surface, and – given knowledge of the volume and surface conductances – relate the trapped charge distribution to the

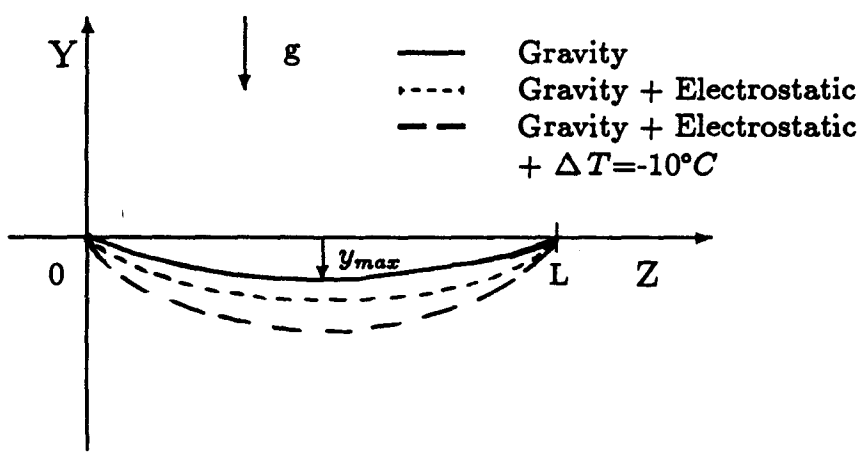

overall ion flux.)

Qualitatively, a scan along the horizontal axis across the bottoms of the sequence of figures shows a systematic shift of the set of equipotential lines to the right as the dielectric constant increases. That is, the "effective width" of the metal strip increases. This shift of the apparent edge of the field-shaping electrode was estimated by matching visually the patterns of the equipotential lines in the vicinity of the dielectric. A much larger sequence of plots than accompany this note – 2 dozen – were actually used for this study. Each plot was compared with the plot obtained using $\epsilon = 1.0$, which corresponds to the vacuum case. The shifts, in mm, were then plotted against the log_{10} of the dielectric constant, shown in Figure 19. This plot clearly shows that below $\epsilon = 0.05$ the "charged-up" surface of the dielectric effectively shields the metal underneath, while above $\epsilon = 8.5$, the fold of dielectric acts as if it were simply additional conductor. Furthermore, the total shift from the vacuum case does not exceed $2.0mm$ in either direction, which roughly corresponds to the mechanical dimensions of the dielectric.

We note finally, from the curve, that when $\epsilon = 2.8$, as for (uncharged) Noryl, the effect is to extend each edge of the metal strip by about $1mm$. Depending upon the degree to which electrons accumulate on the Noryl surface, one may thus estimate that the plastic strip holders introduce an uncertainty in the strip width of roughly $+1mm/-2mm$. The impact of these variations upon the tube drift characteristics are readily extracted for these various cases.

9. Isochrones, Drift Lines & Spring Constants : $90\mu m$ wire

In section 4, we presented results concerning a 75 μm sense wire. A similar description can be given for a 90 μm sense wire (Figures 20-32). These figures parallel Figures 1–10 and are self-explanatory.

For this particular wire, we studied the effects of wire displacements for four different voltage combinations on the anode and field shaping electrodes. Tables 1 through 4 give a detailed listing of the results for these 4 different voltage combinations. Included are the "spring constants", k_E, for displacements parallel (left-right) and perpendicular (up-down) to the drift direction, the critical "wavelength", b, determining the stability, and the worst-case displacement when gravity combines with electrostatic forces under $1000gm$ tension. In the calculations, we used the following:

$1dyne = 1 \times 10^{-5}$ N
Diameter of the wire = 90 μm
$f_G = 1.228 dyn/cm$
Gravitational sag $y_G = -0.131 \times 10^{-2}\ m$
$L = 9\ m$
$T_F = 952.6 \times 10^3\ dynes = 9.526$ N

Table 1

Anode voltage = 6000 volts
field shaping voltage = 6000 volts

direction	F N	disp m	k_E dyn/cm^2	b m	y_G+y_E m
up	-0.189×10^{-3}	2×10^{-3}	-0.943		0.120×10^{-2}
down	0.189×10^{-3}	-2×10^{-3}	-0.944		0.120×10^{-2}
left	-0.259×10^{-3}	-2×10^{-3}	1.3	53.9	-0.147×10^{-2}
right	0.261×10^{-3}	2×10^{-3}	1.3	53.7	-0.148×10^{-2}

Table 2

Anode voltage = 5500 volts
field shaping voltage = 5000 volts

direction	F N	disp m	k_E dyn/cm^2	b m	y_G+y_E m
up	-0.158×10^{-3}	2×10^{-3}	-0.789		0.122×10^{-2}
down	0.158×10^{-3}	-2×10^{-3}	-0.790		0.122×10^{-2}
left	-0.216×10^{-3}	-2×10^{-3}	1.08	59.0	-0.144×10^{-2}
right	0.218×10^{-3}	2×10^{-3}	1.09	58.8	-0.144×10^{-2}

Table 3

Anode voltage = 5000 volts
field shaping voltage = 4000 volts

direction	F N	disp m	k_E dyn/cm^2	b m	y_G+y_E m
up	-0.126×10^{-3}	2×10^{-3}	-0.628		0.124×10^{-2}
down	0.126×10^{-3}	-2×10^{-3}	-0.628		0.124×10^{-2}
left	-0.173×10^{-3}	-2×10^{-3}	0.864	66.0	-0.141×10^{-2}
right	0.175×10^{-3}	2×10^{-3}	0.873	65.7	-0.141×10^{-2}

Table 4

Anode voltage = 4500 volts
field shaping voltage = 3000 volts

direction	F N	disp m	k_E dyn/cm^2	b m	y_G+y_E m
up	-0.916×10^{-4}	2×10^{-3}	-0.458		0.125×10^{-2}
down	0.917×10^{-4}	-2×10^{-3}	-0.458		0.125×10^{-2}
left	-0.130×10^{-3}	-2×10^{-3}	0.650	76.1	-0.139×10^{-2}
right	0.132×10^{-3}	2×10^{-3}	0.659	75.5	-0.139×10^{-2}

These results are strongly constrained by the laws of electrostatics. A study of the capacitance coefficients leads to a simple parametrization which may be written in the form

$$k_E = A \cdot \left[1 - \delta(1-R)^2\right] \cdot V_A^2, \tag{6}$$

where $V_A(Volts)$ is the Anode (wire) potential, R is the ratio of the field-shaping electrode potential to V_A, and k_E is in N/m^2. The parameters A and δ depend only upon the electrode geometry (including the wire diameter) and, from our results in Tables 1-4, we may estimate them to be:

$$A_{lr} = 3.61 \times 10^{-9} farad\ m^{-3}, \quad \delta_{lr} = 1.00$$

for displacements parallel to the drift direction (left-right), and

$$A_{ud} = -2.62 \times 10^{-9} farad\ m^{-3}, \quad \delta_{ud} = 1.23$$

transversely (up-down). (These A and δ constants should improve over time as the SDC muon tube design becomes better determined and analyzed!)

10. Summary

We have studied the $9cm$ drift tube with a $75\mu m$ diameter wire and the field-shaping electrode both at 6.5kV and also with the latter at 5.5kV. We found out that for the first case linearity holds to within $160\mu m$, whereas for the second it improves to within $80\mu m$. The shifting of the wire by $2mm$ up or down does not have much effect on the effective track position measurement. On the other hand, on shifting the wire $2mm$ left/right, the inferred track position is displaced by about 20% less than the actual wire shift. The electrostatic forces are found to alter significantly the figure of a wire sagging under gravity. Also, for temperature fluctuations of $\pm 10°C$, there will be a uncertainty in measurement precision of as much as $160\mu m$, in the worst

case. In addition, the effects of the dielectric holders of the field-shaping electrodes are described.

The analyses are repeated for a $90\mu m$ diameter wire and several potential combinations, and similar results are obtained. A simple parametrization of the "spring constants" characterizing the electrostatic forces is obtained.

APPENDIX I : Electrostatic Simulation

The CERN Library program "POISSON" was used for the basic electrostatic potential calculations. This system uses a finite-element solution of Laplace's Equation and, although developed primarily for magnet calculations, it handles electrostatic boundary conditions at dielectrics very nicely also. Operating in a sequence of steps, a program "LATTCR" first converts an input file defining the various regional boundaries and their potentials and other characteristics into an optimized lattice of small triangles – the mesh at whose vertices the electric potential is to be calculated. The second program, "POISCR", executes the equation solution by a relaxation process and fills in the potentials at all the mesh points, both those on the boundaries and those within the several regions, and writes the result to a large file which also contains information defining the regions and the various other parameters. In the CERN version the third POISSON program, "TRIPCR", then reads this large file and prepares the display of the resulting potential distribution using HIGZ graphics calls. The POISSON system has a large number of adjustable input parameters almost all of which, except for those actually defining the regional geometry and boundary conditions, are defaulted with the possibility of selective alteration by using Fortran "NAMELIST" entries in the command file invoking the several programs. These include a number of switches which cause POISCR to calculate field components and other derived data, and others which induce TRIPCR to display the unoptimized and optimized triangular lattices, for the curious.

For our present purposes the last POISSON routine, TRIPCR was modified in its operation on the potential distribution file presented by POISCR; the new program was dubbed "TIMPLOT". The primary amendment was the introduction of a locally written electric field-line generator which "SWIMS" down the potential gradient, opposite the electron drift direction, and thus plots the electric field lines. The "swimming" is based upon finding the direction for a given incremental length of chord (small!) which makes equal angles with the electric field (as calculated by a Poisson routine) at the chord end points. This process starts near the sense wire and proceeds until an electrode boundary is struck – or occasionally until it takes too many iterations (eg. 20) to find the best chord at which point the routine gives up and the trajectory is "lost". This happens rarely, if the chosen increment is small enough and is associated with end points lying too near a mesh line so that the set of mesh points participating in the field calculation becomes indeterminate. This

penalty for using finite element methods can be ameliorated by using finer increments – and more time. Electron drift-timing is done out from the initial trajectory point and is based upon a Fortran function containing interpolating look-up tables of the drift velocities vs field made from reported data for various gases of interest. Finally, a rather arbitrary additional increment to the drift time is estimated for the interval between the starting point of the above trajectory and the sense wire. The individual trajectories which are propagated out from the sense wire are defined by a set of azimuthal angles. These angles, the starting radius and other relevant parameters for TIMPLOT execution are defined, as with the rest of the POISSON system, by an input NAMELIST.

To display and record the above calculations TIMPLOT has a number of facilities, in addition to those of its parent TRIPCR, including the capacity to produce displays on-screen, or by Postscript Metafile.

As each trajectory propagates out along a field line it notes the passage of $50nsec$ with an "$*$" and of $250nsec$ with a "o". (These displays are easily alterable.) Further, the routine outputs onto a formatted Fortran file an "event" record each time the trajectory reaches a periodic set of lines perpendicular to the mean drift direction ("x") which simulate the passage of an ionizing track. This line may, moreover, be tilted from perpendicularity by an arbitrary angle. Recorded in each case are eight parameters : the azimuthal angle defining the trajectory, the track-tilt angle just mentioned, the x-coordinate defining the track, the y-coordinate of the trajectory intersection, the drift time at that point, the electric potential and the field magnitude at that point, and the drift velocity associated with that field. This output file of events can be listed directly. Much more conveniently, with a simple auxilliary program, caller "APTUPLE", it can be converted to a direct-access ZEBRA-file HBOOK NTUPLE for further analysis by the PAW system. This has proven very useful, as illustrations in this report will witness.

A final feature of TIMPLOT, which we have little exploited so far, is its ability to generate via HIGZ a "picture" file in RZ format, for further editing via PAW.

The program WIRECAP, used to calculate the electrostatic forces on the wire and also the wire potentials, is a similar adaptation of POISSON which uses the POISSON-generated potential distribution along with the POISSON routines which calculate the electric field and field-gradient tensor components. To check the operation of these routines, a detailed study was made of the electrostatic force upon a small cylinder ($2mm$ radius to simulate our drift chamber studies) contained eccentrically within a larger one of diameter $9cm$. This problem can be solved exactly, using images. The comparison between the POISSON "measured" spring constants and the exactly calculated values is shown in Figure 33 which illustrates agreement to within about 4 percent over a displacement range of $30mm$ – nearly the full tube radius.

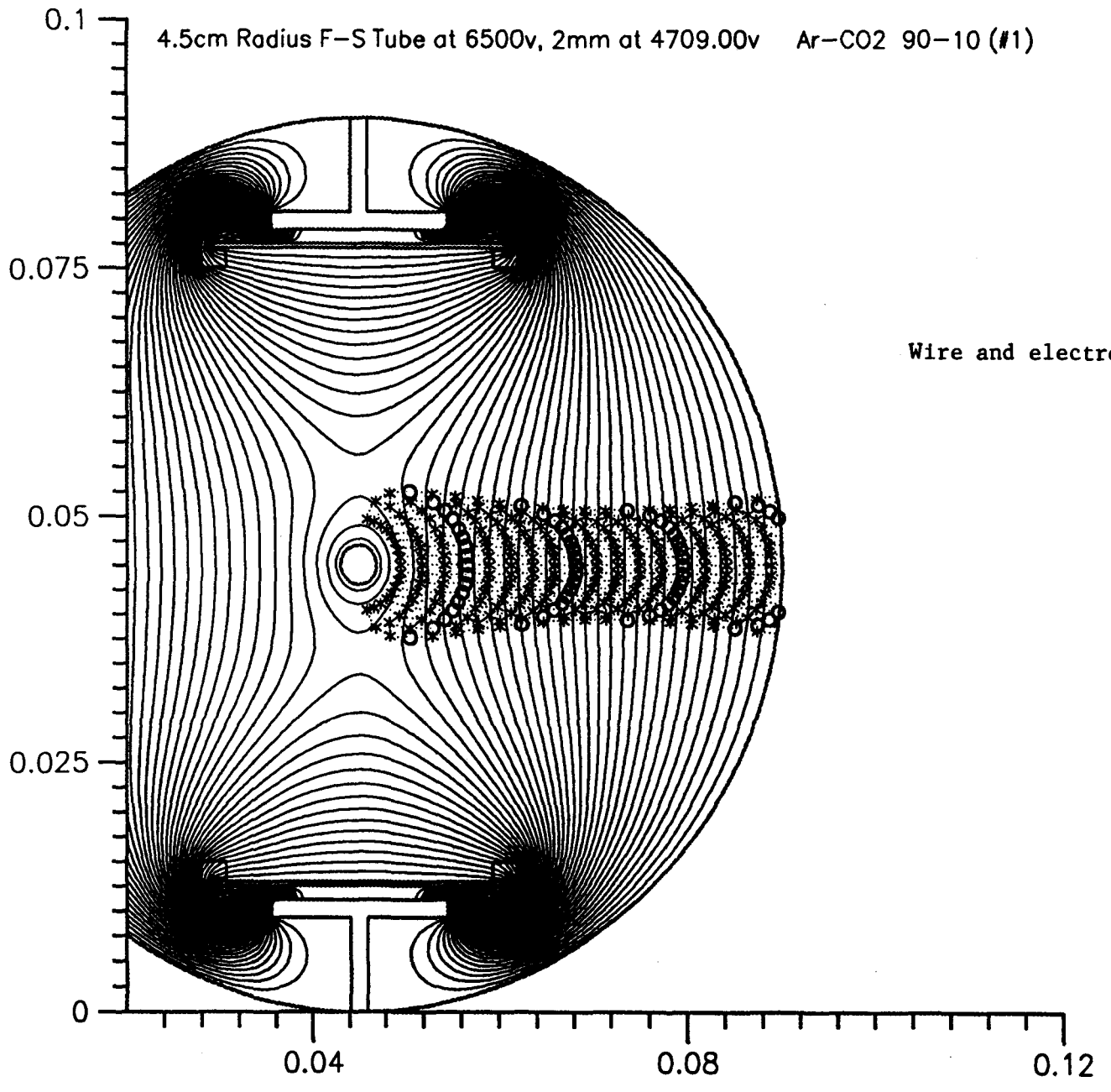

Wire and electrode at 6500 volts

Fig. 1

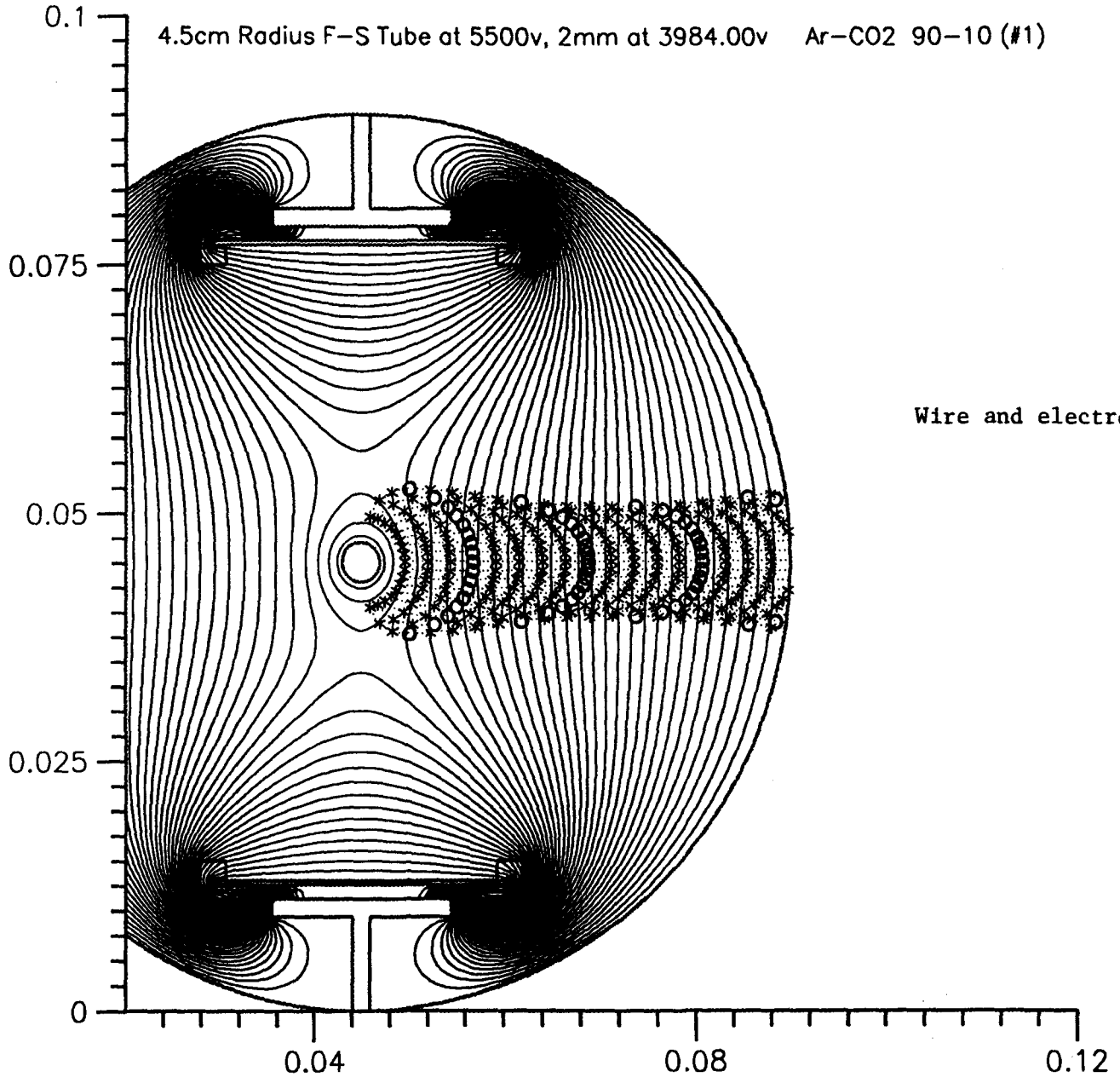

Wire and electrode at 5500 volts

Fig. 2

Fig. 3

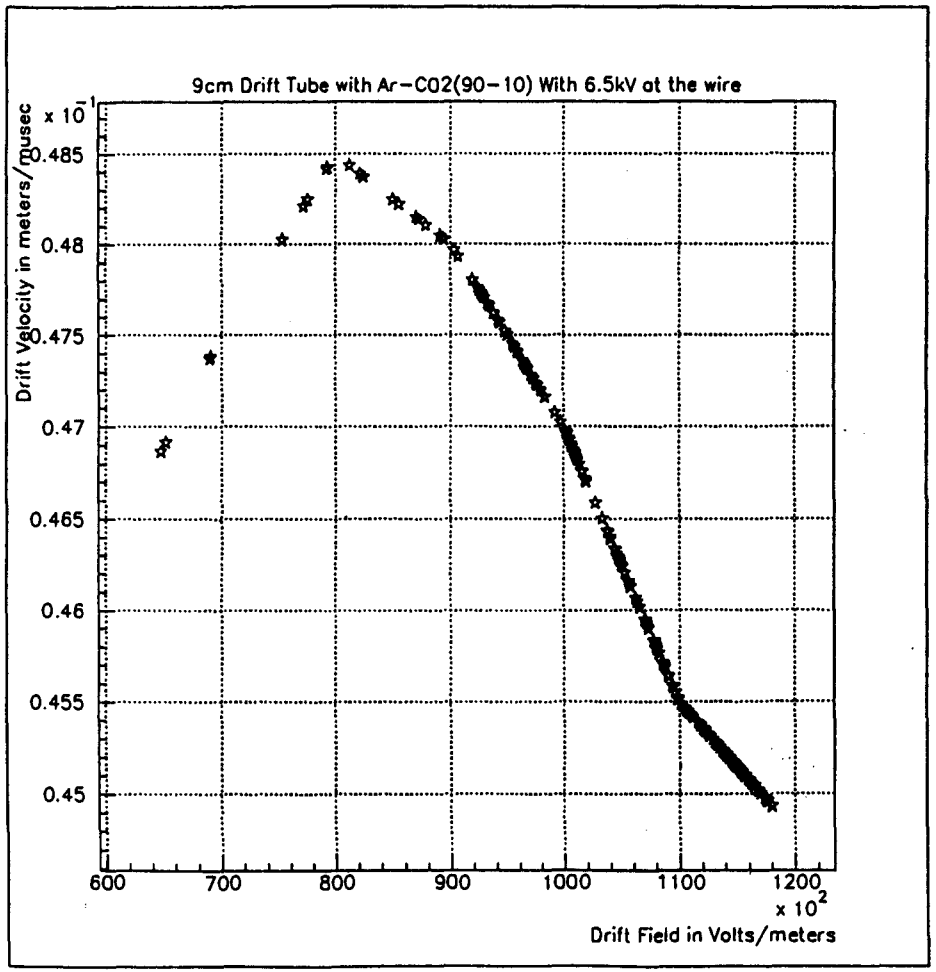
9cm Drift Tube with Ar−CO2(90−10) With 6.5kV at the wire
Drift Velocity in meters/musec
x 10^-1
0.485
0.48
0.475
0.47
0.465
0.46
0.455
0.45
600
700
800
900
1000
1100
1200
x 10^2
Drift Field in Volts/meters

Fig. 4

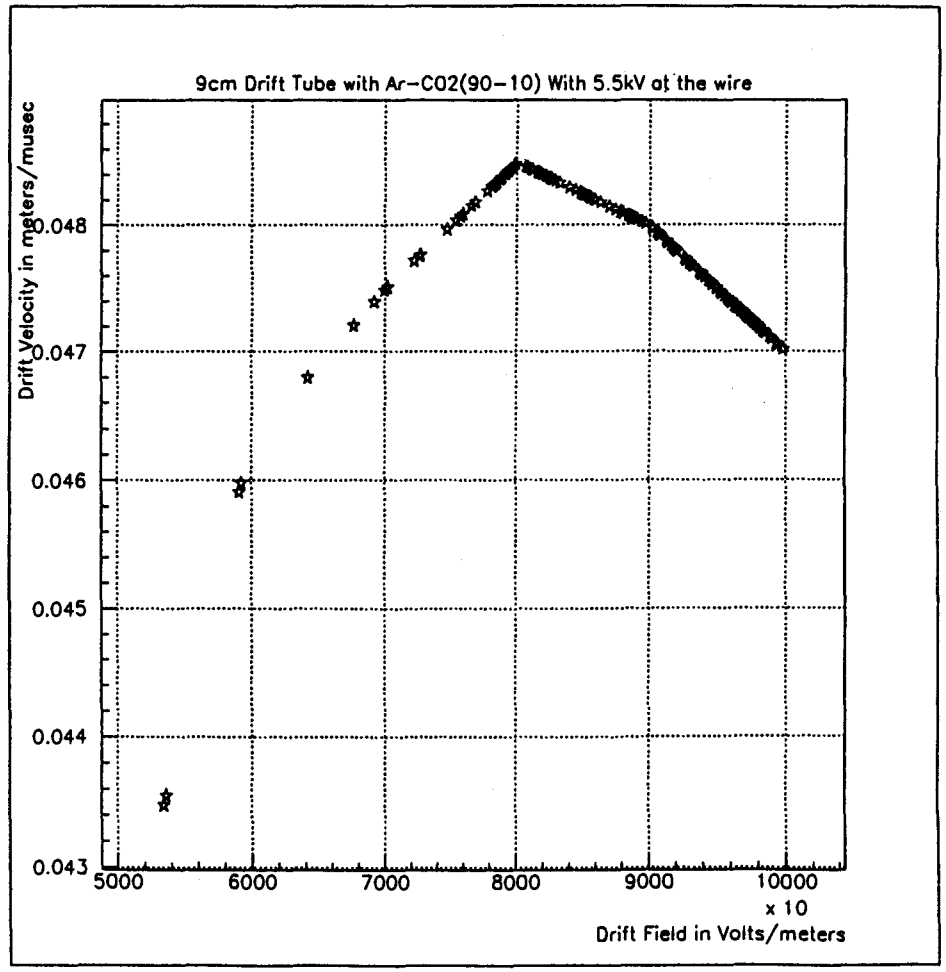
9cm Drift Tube with Ar−CO2(90−10) With 5.5kV at the wire
Drift Velocity in meters/musec
0.048
0.047
0.046
0.045
0.044
0.043
5000
6000
7000
8000
9000
10000
x 10
Drift Field in Volts/meters

Fig. 5

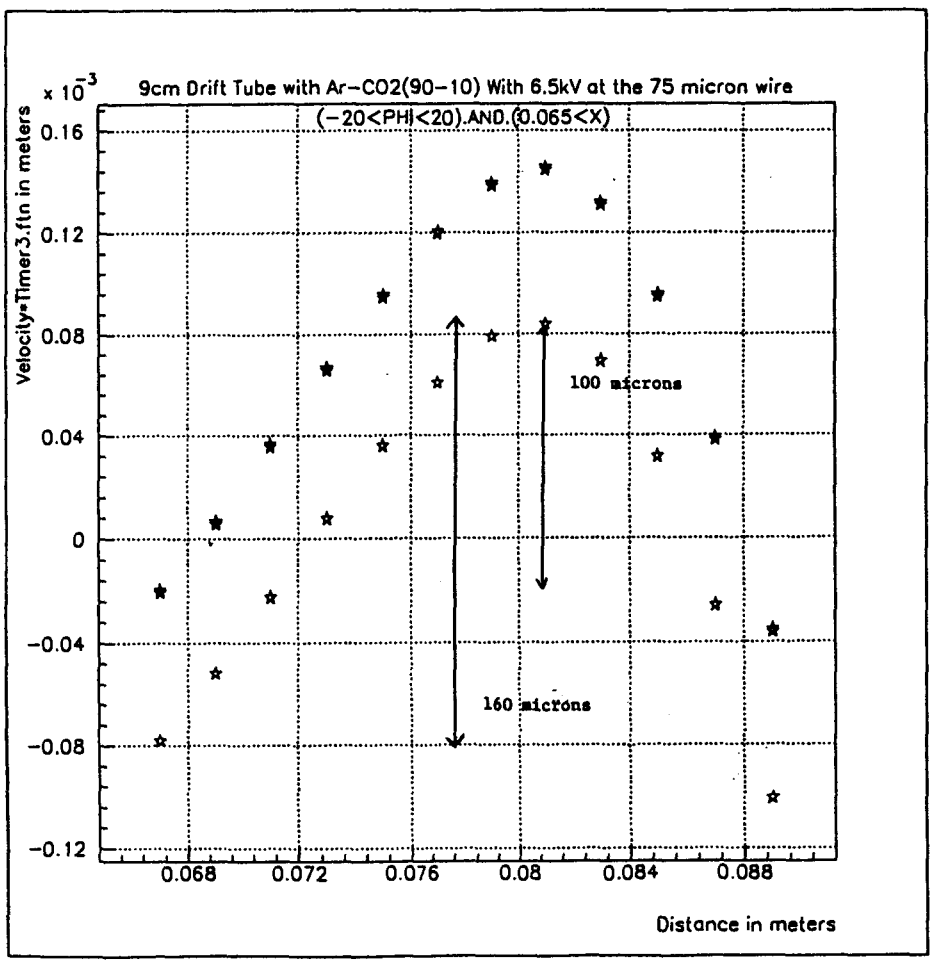
9cm Drift Tube with Ar−CO2(90−10) With 6.5kV at the 75 micron wire
(−20<PHI<20).AND.(0.065<X)
x 10^-3
Velocity*Timer3.ftn in meters
0.16
0.12
0.08
0.04
0
−0.04
−0.08
−0.12
0.068
0.072
0.076
0.08
0.084
0.088
100 microns
160 microns
Distance in meters

Fig. 6

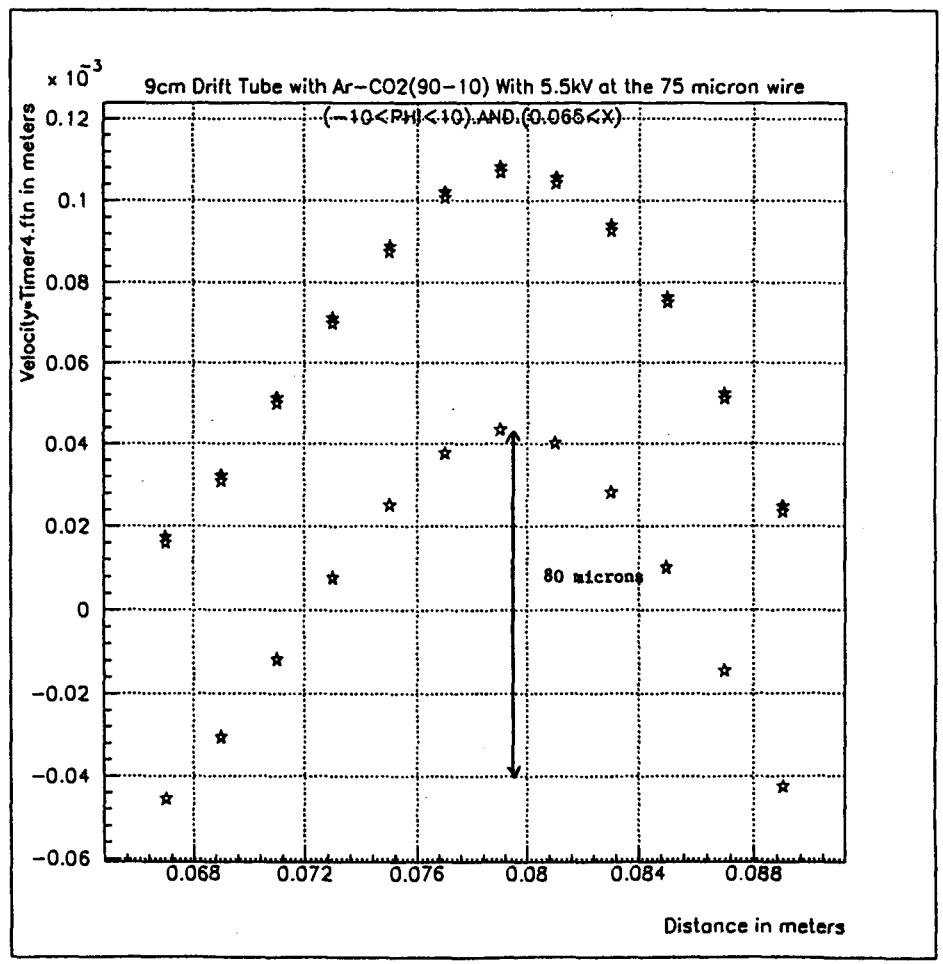
9cm Drift Tube with Ar−CO2(90−10) With 5.5kV at the 75 micron wire
(−10<PHI<10).AND.(0.066<X)
x 10^-3
Velocity*Timer4.ftn in meters
0.12
0.1
0.08
0.06
0.04
0.02
0
−0.02
−0.04
−0.06
0.068
0.072
0.076
0.08
0.084
0.088
80 microns
Distance in meters

Fig. 7

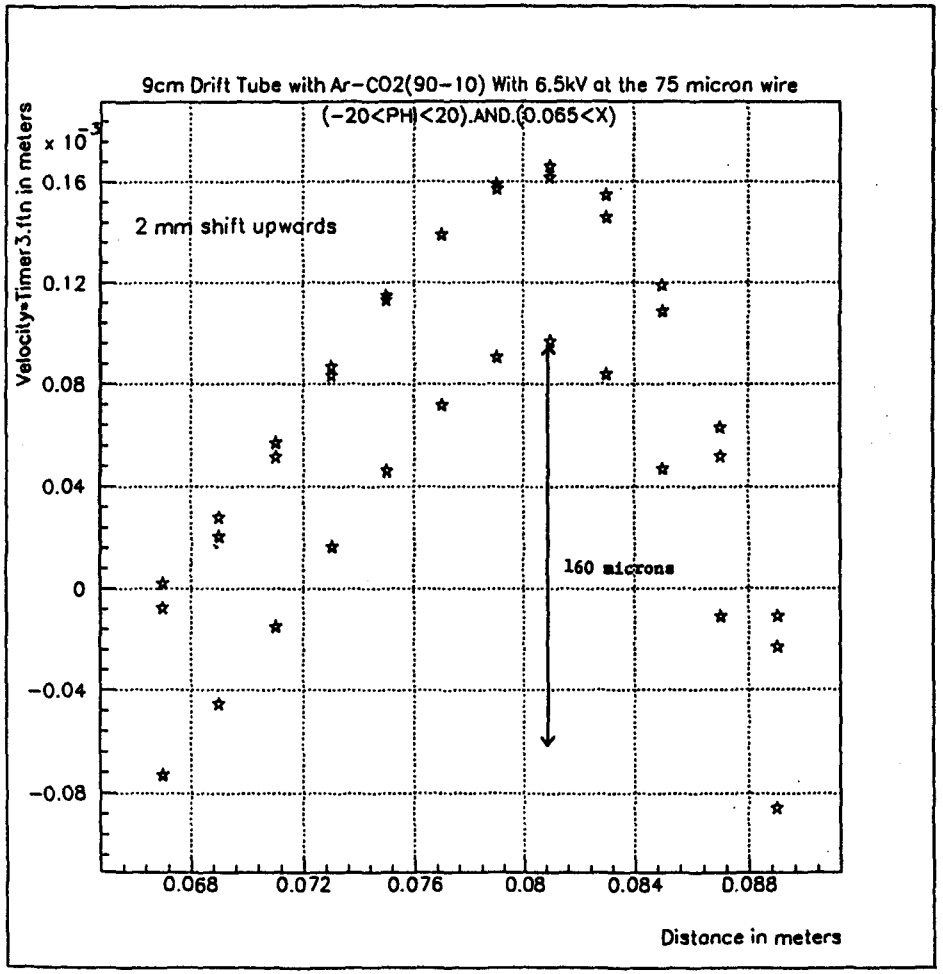
9cm Drift Tube with Ar-CO2(90-10) With 6.5kV at the 75 micron wire
(-20<PHI<20).AND.(0.065<X)
2 mm shift upwards
160 microns
Velocity*Timer3.ftn in meters
x 10^-3
0.16
0.12
0.08
0.04
0
-0.04
-0.08
0.068
0.072
0.076
0.08
0.084
0.088
Distance in meters

Fig. 8

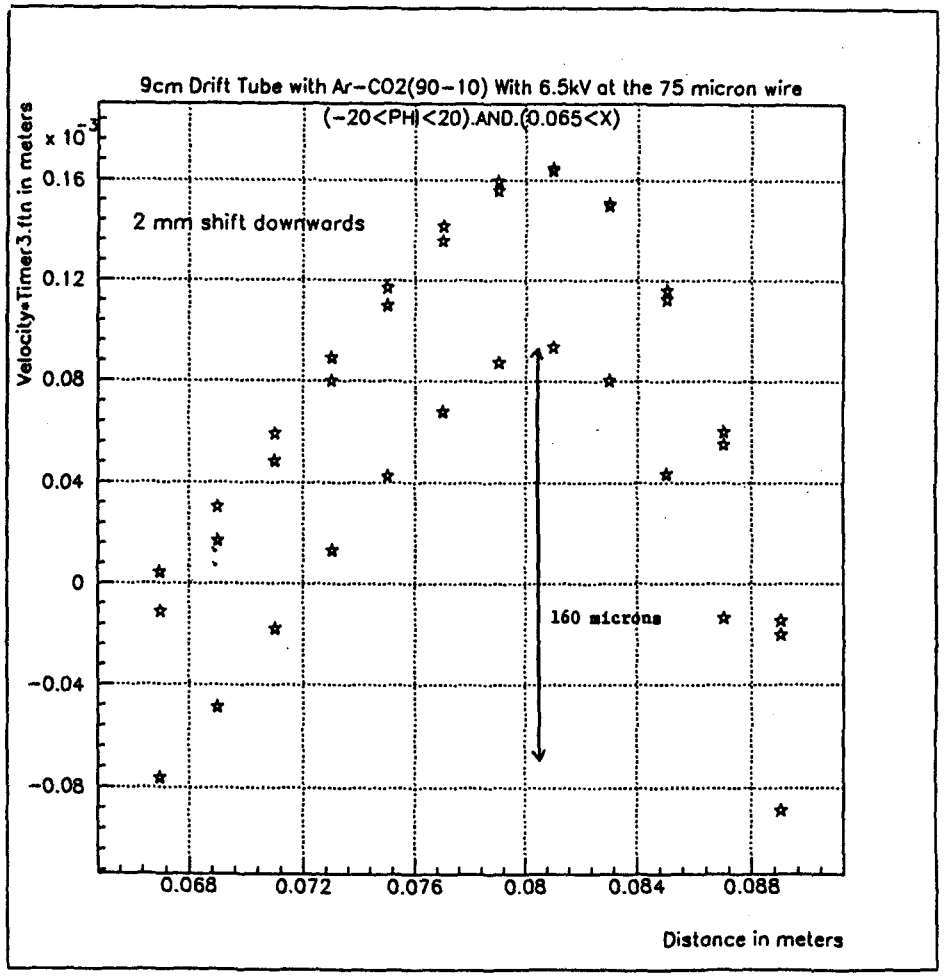
9cm Drift Tube with Ar-CO2(90-10) With 6.5kV at the 75 micron wire
(-20<PHI<20).AND.(0.065<X)
2 mm shift downwards
160 microns
Velocity*Timer3.ftn in meters
x 10^-3
0.16
0.12
0.08
0.04
0
-0.04
-0.08
0.068
0.072
0.076
0.08
0.084
0.088
Distance in meters

Fig. 9

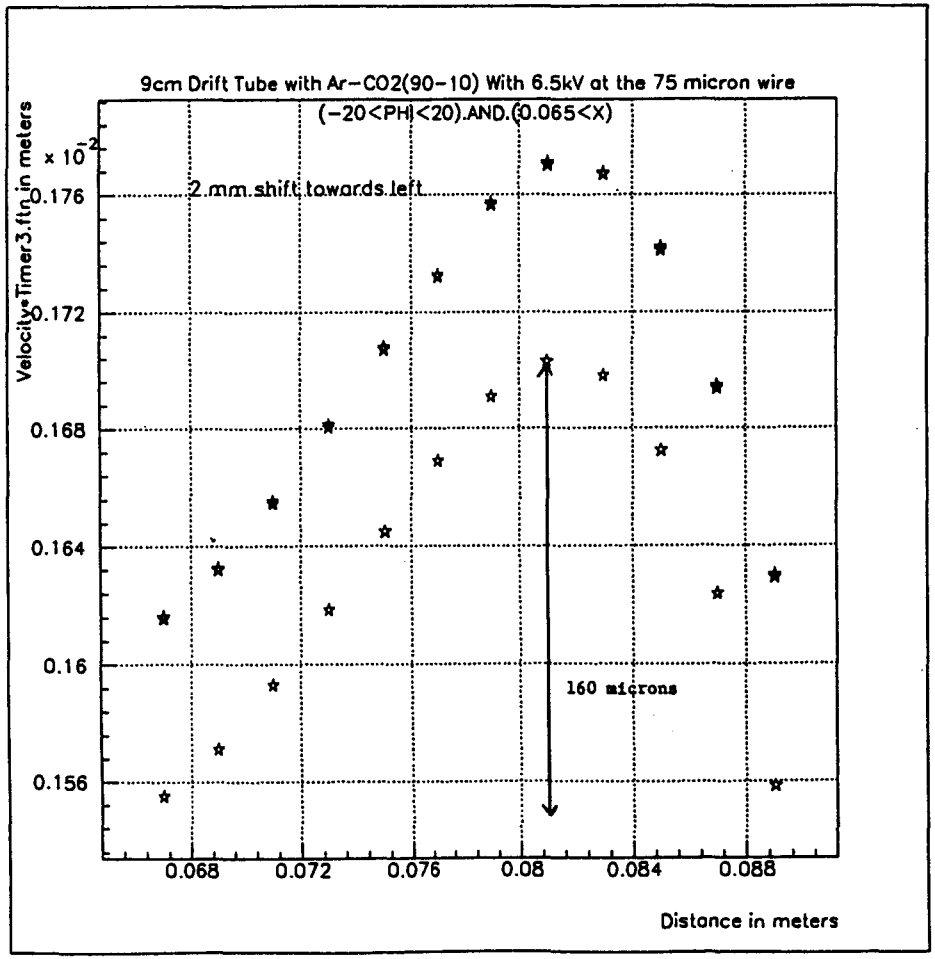
9cm Drift Tube with Ar−CO2(90−10) With 6.5kV at the 75 micron wire
(−20<PH<20).AND.(0.065<X)
2 mm shift towards left
160 microns
Velocity*Timer3.ftn in meters
x 10^-2
0.176
0.172
0.168
0.164
0.16
0.156
0.068
0.072
0.076
0.08
0.084
0.088
Distance in meters

Fig. 10

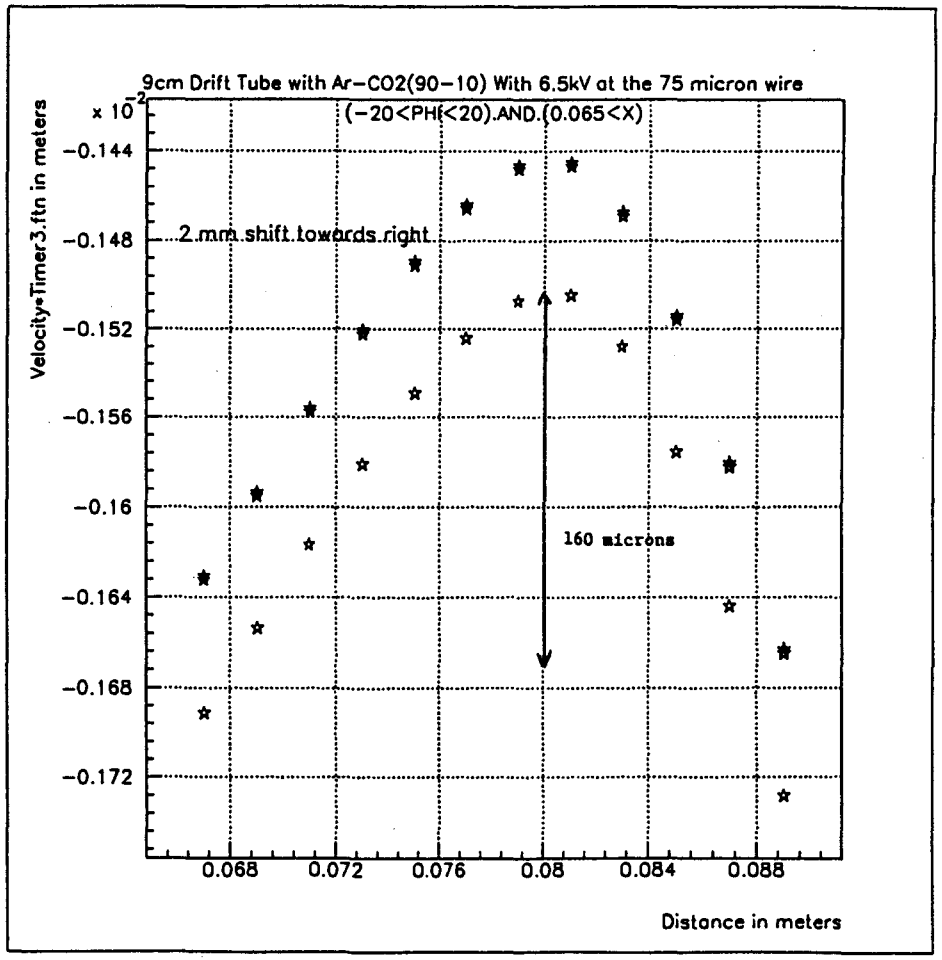
9cm Drift Tube with Ar−CO2(90−10) With 6.5kV at the 75 micron wire
(−20<PH<20).AND.(0.065<X)
2 mm shift towards right
160 microns
Velocity*Timer3.ftn in meters
x 10^-2
−0.144
−0.148
−0.152
−0.156
−0.16
−0.164
−0.168
−0.172
0.068
0.072
0.076
0.08
0.084
0.088
Distance in meters

27 JAN 1964
KOCHOCKI
McMASTER
OLIVER

GOLD-PLATED TUNGSTEN WIRE
(0.002 inch diameter)

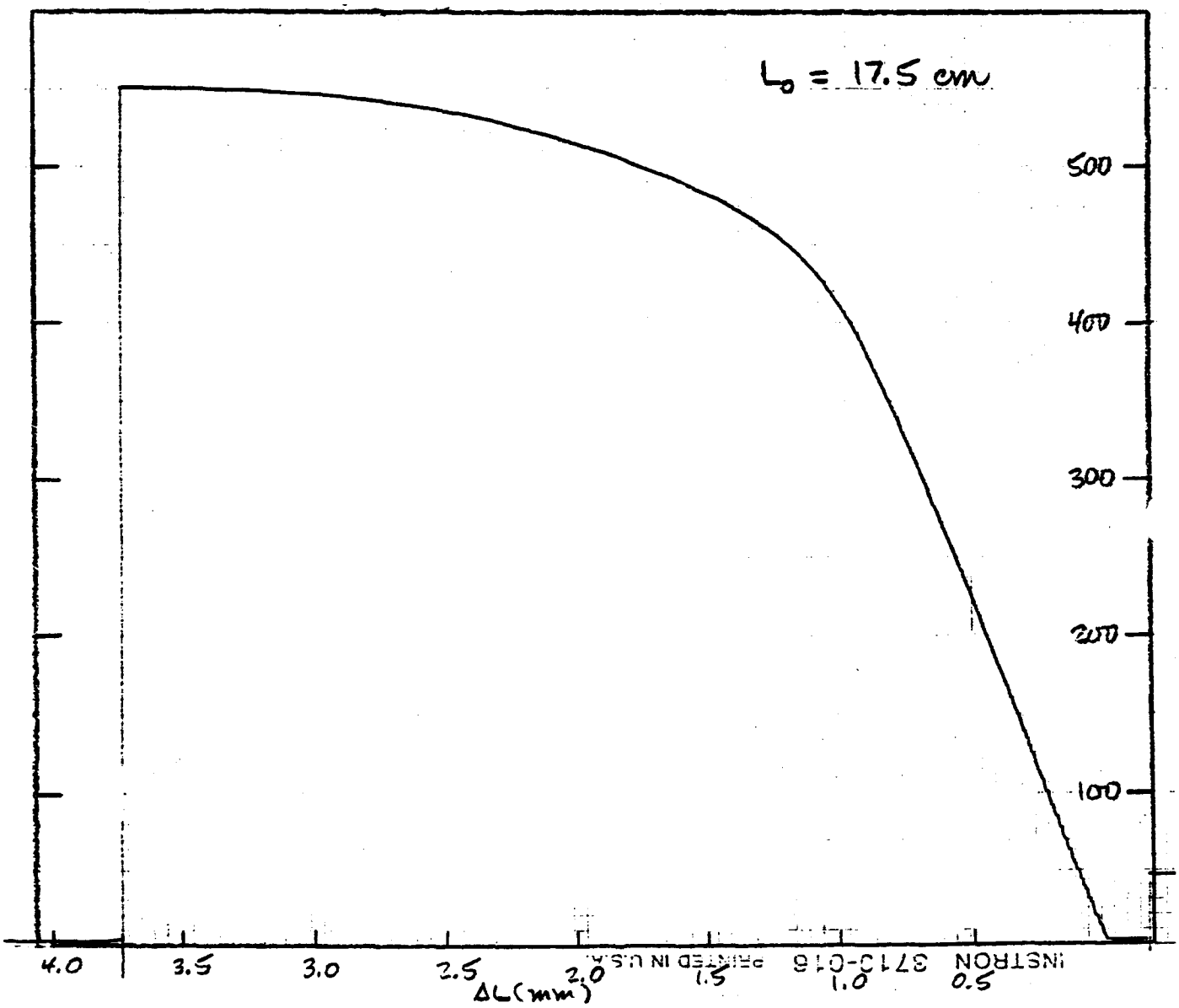

Fig. 11

Fig. 12

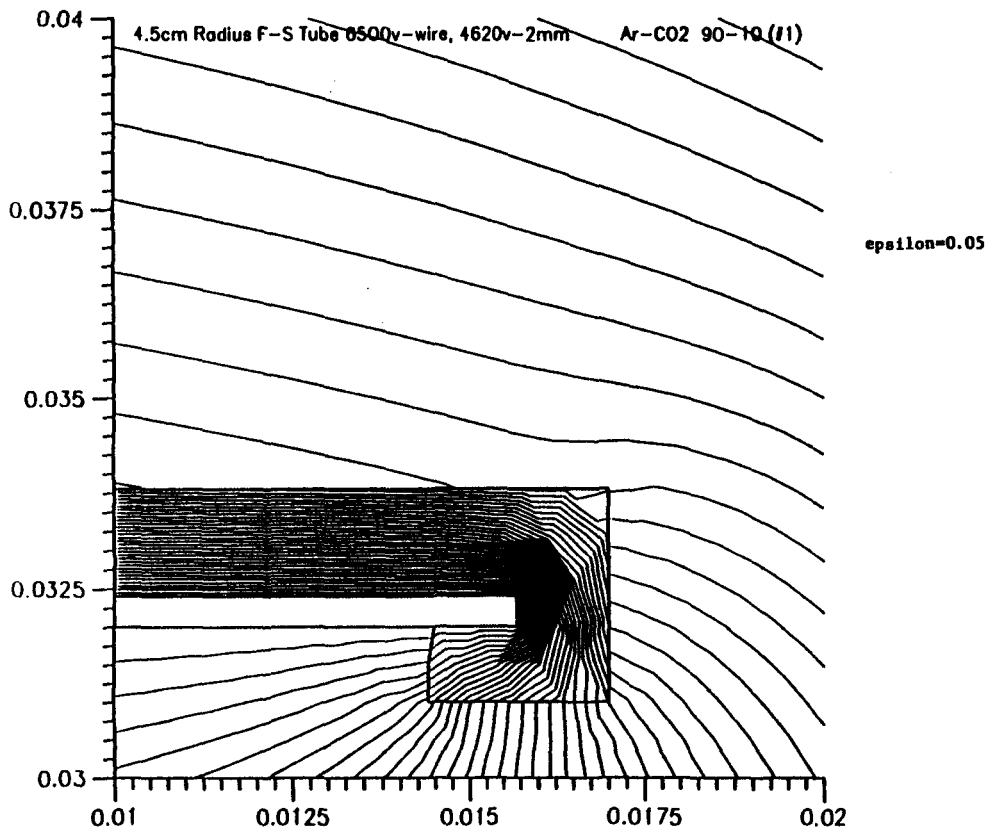
4.5cm Radius F-S Tube 6500v-wire, 4620v-2mm
Ar-CO2 90-10 (I1)
epsilon=0.05
0.04
0.0375
0.035
0.0325
0.03
0.01
0.0125
0.015
0.0175
0.02

Fig. 13

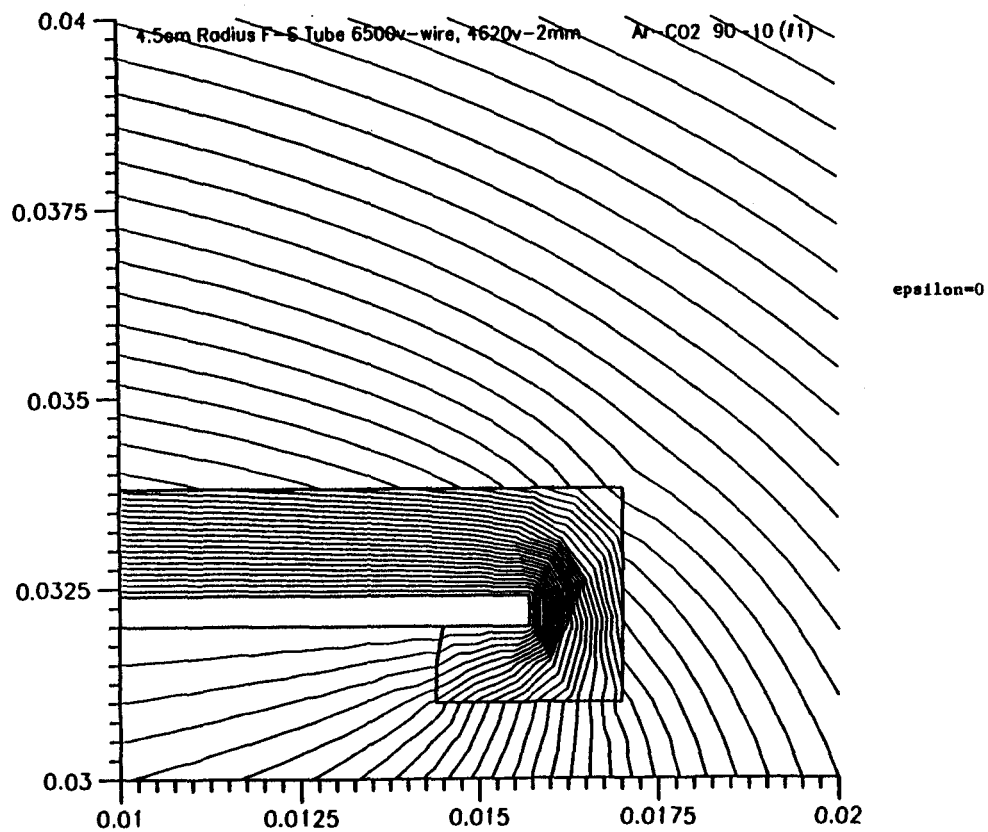
4.5cm Radius F-S Tube 6500v-wire, 4620v-2mm
Ar-CO2 90-10 (I1)
epsilon=0
0.04
0.0375
0.035
0.0325
0.03
0.01
0.0125
0.015
0.0175
0.02

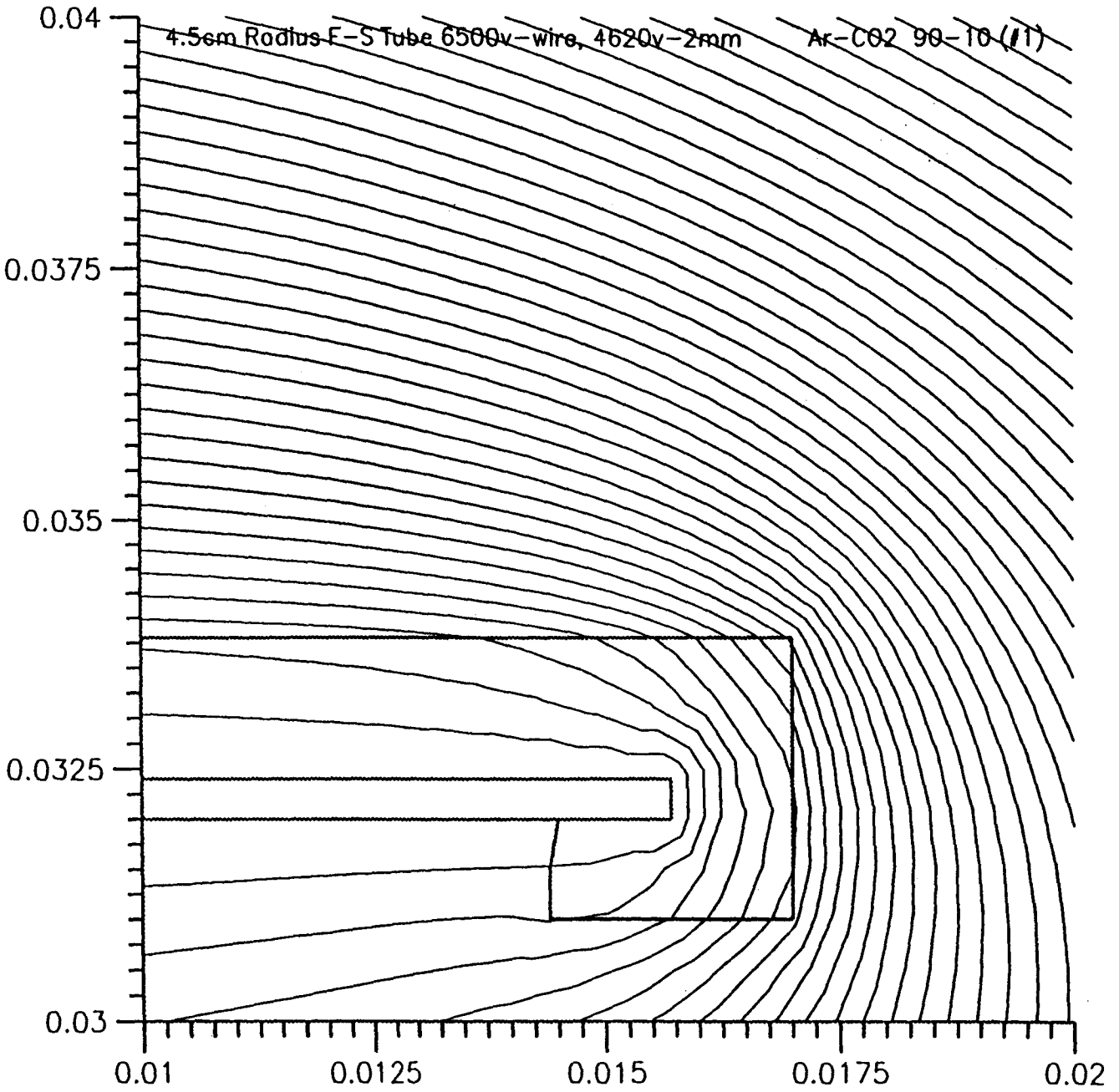

epsilon=2.8

Fig. 14

Fig. 15

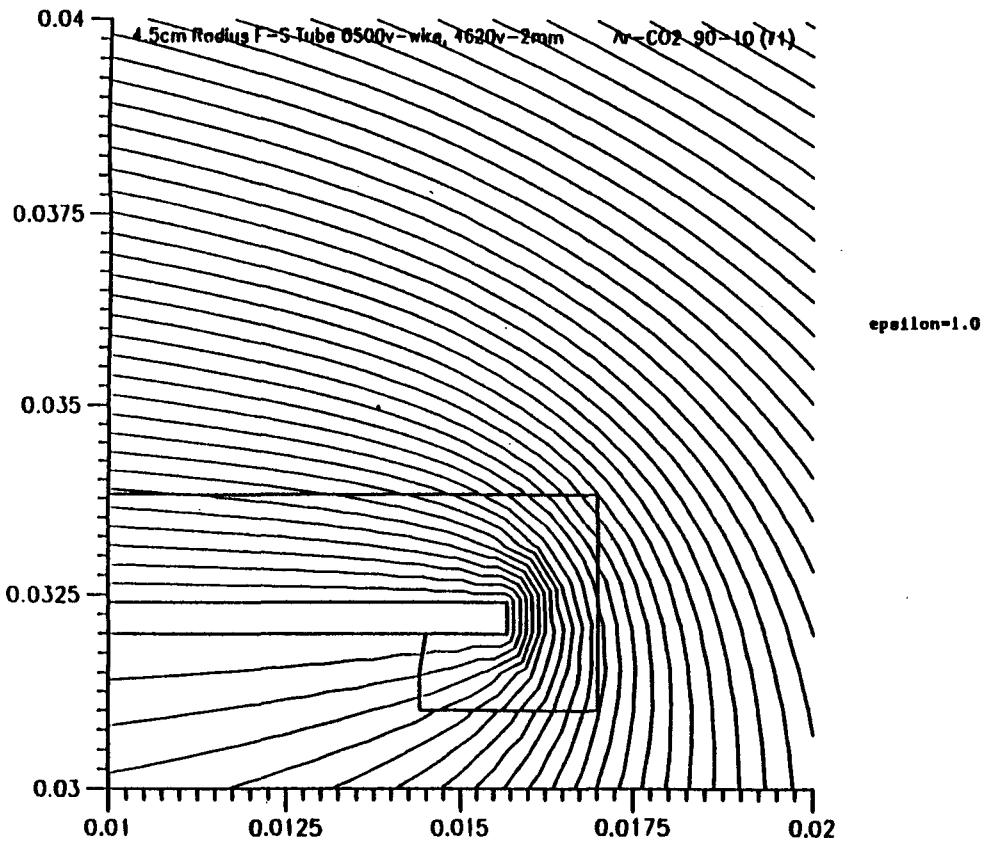
4.5cm Radius F-S Tube 6500v-wire, 4620v-2mm
Ar-CO2 90-10 (T1)
0.04
0.0375
0.035
0.0325
0.03
0.01
0.0125
0.015
0.0175
0.02
epsilon=1.0

Fig. 16

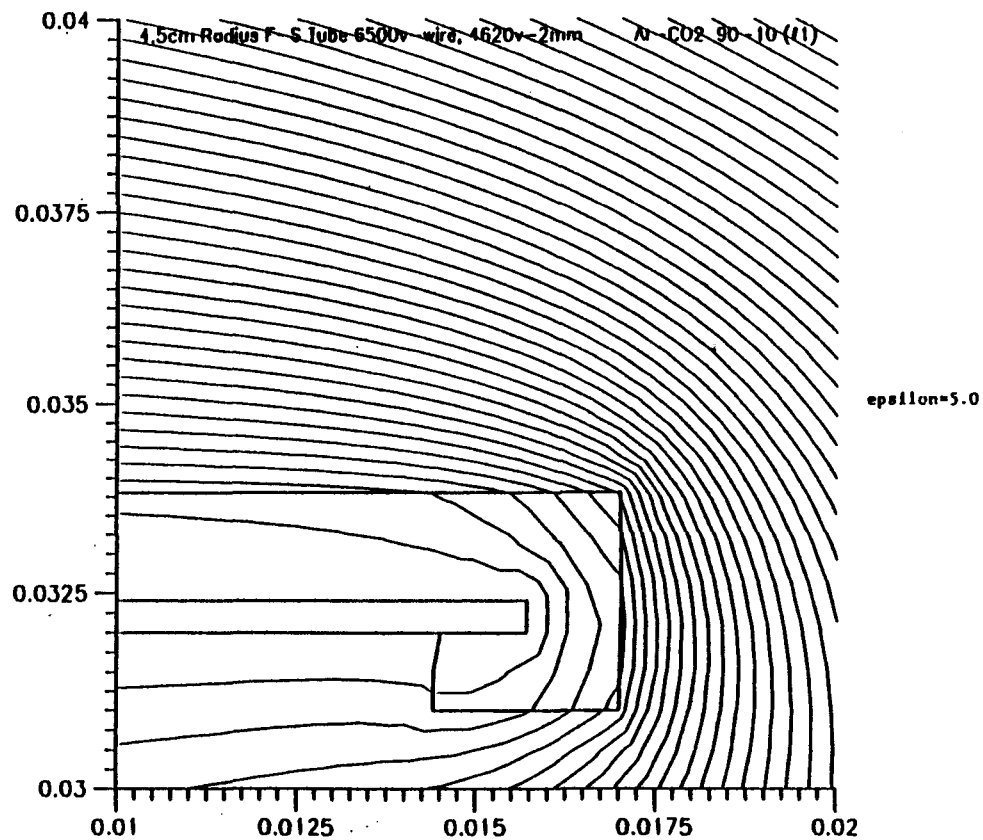
4.5cm Radius F-S Tube 6500v-wire, 4620v-2mm
Ar-CO2 90-10 (T1)
0.04
0.0375
0.035
0.0325
0.03
0.01
0.0125
0.015
0.0175
0.02
epsilon=5.0

Fig. 17

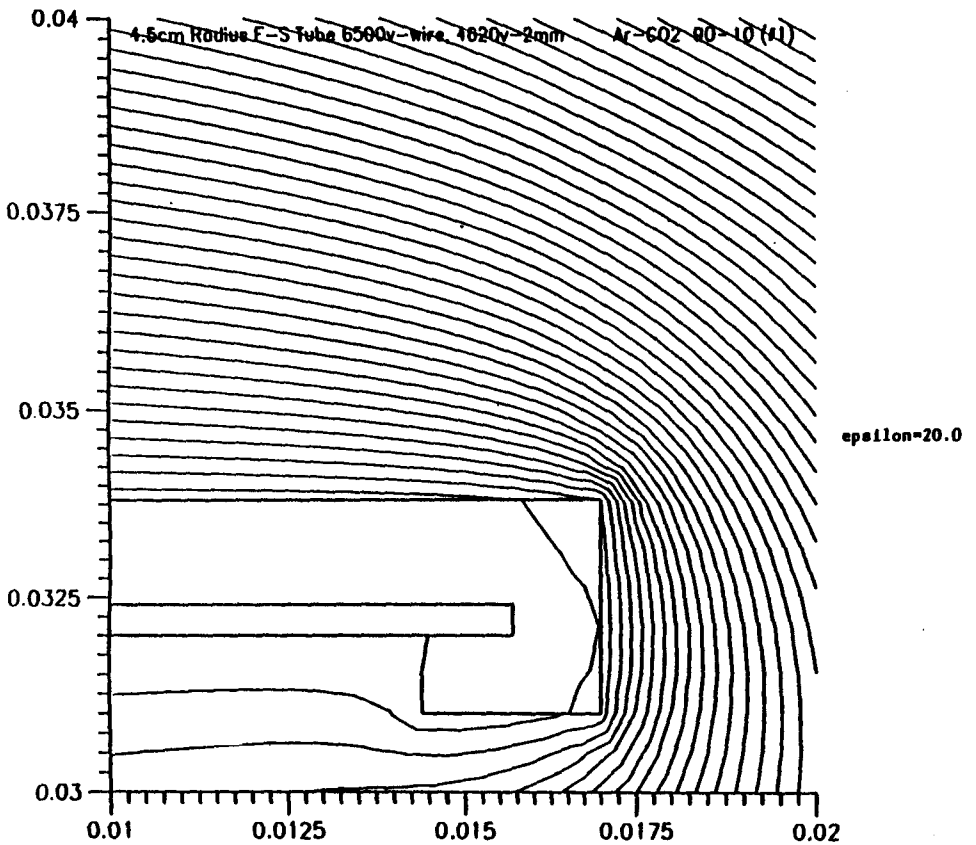
4.5cm Radius F-S Tube 6500v-wire, 4620v-2mm
Ar-CO2 90-10 (#1)
epsilon=20.0
0.04
0.0375
0.035
0.0325
0.03
0.01
0.0125
0.015
0.0175
0.02

Fig. 18

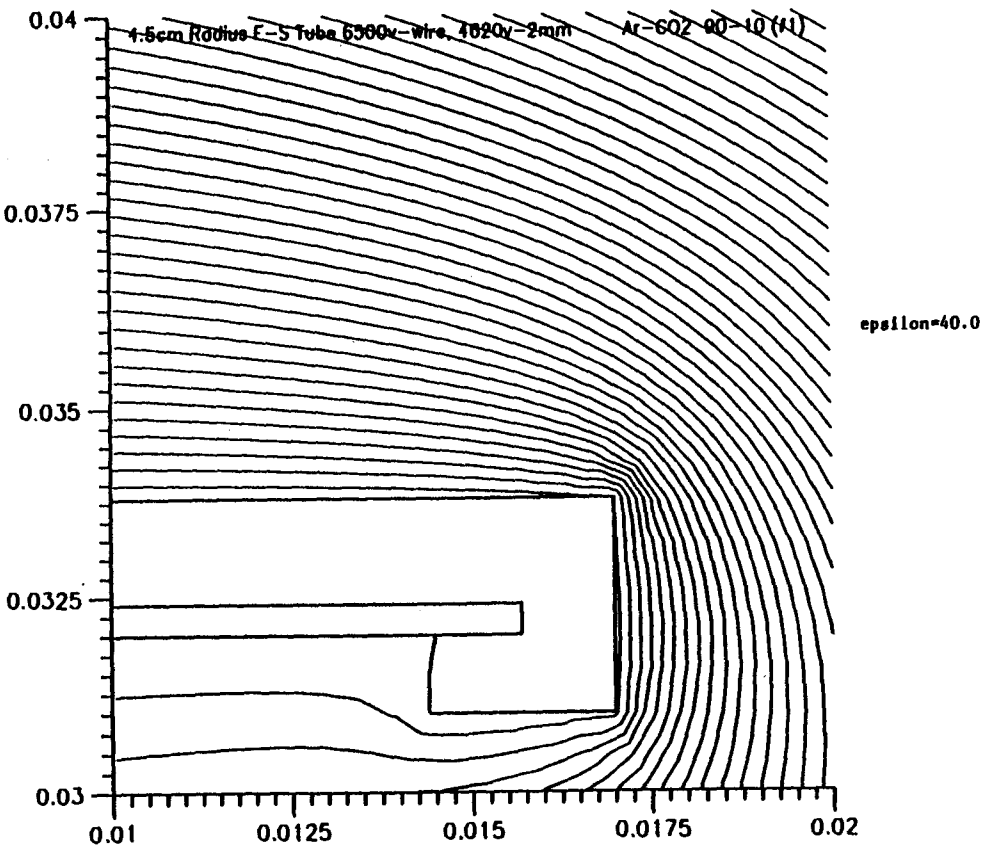
4.5cm Radius F-S Tube 6500v-wire, 4620v-2mm
Ar-CO2 90-10 (#1)
epsilon=40.0
0.04
0.0375
0.035
0.0325
0.03
0.01
0.0125
0.015
0.0175
0.02

Fig. 19

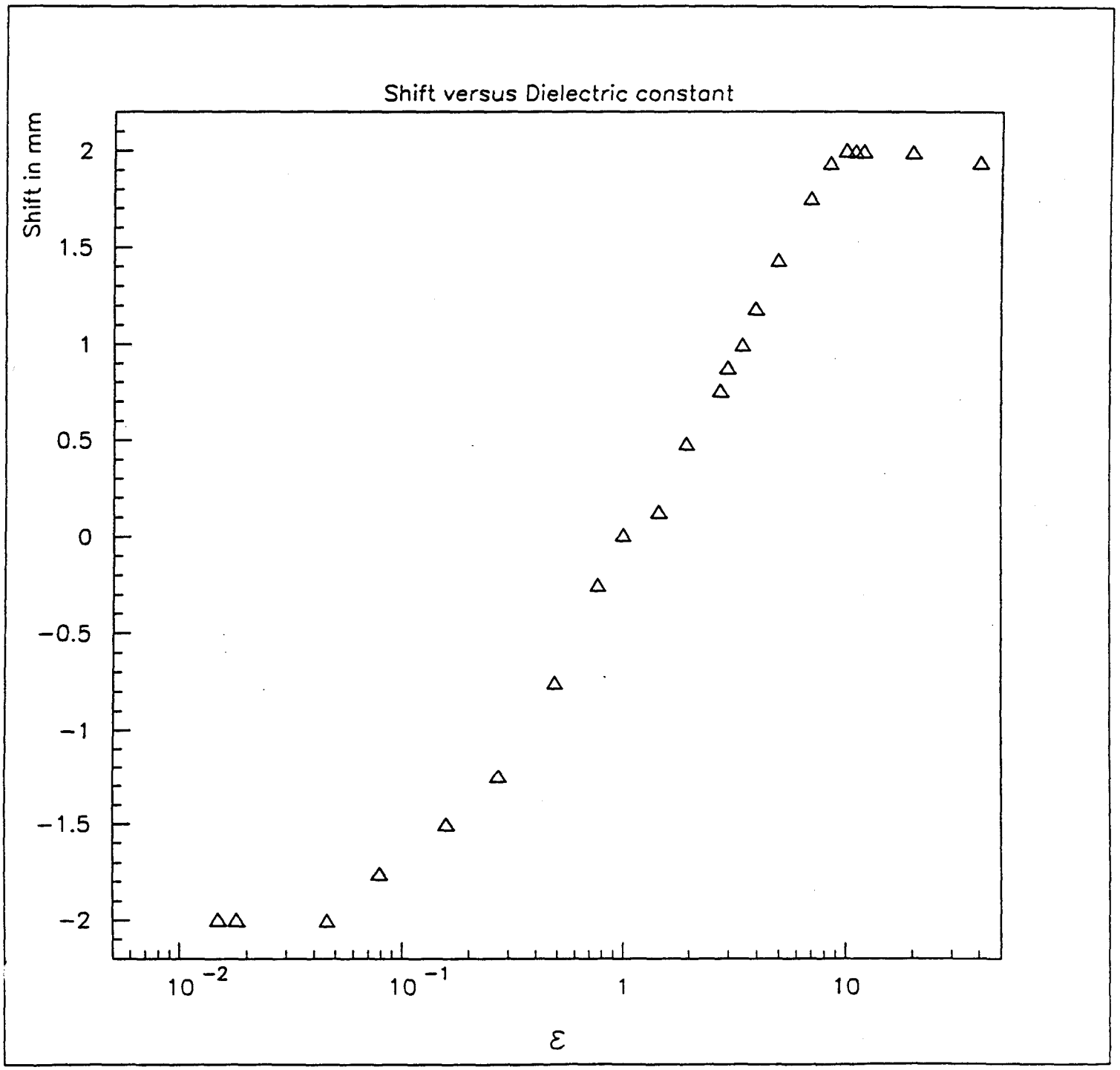
Shift versus Dielectric constant
Shift in mm
2
1.5
1
0.5
0
−0.5
−1
−1.5
−2
10 −2
10 −1
1
10
ε

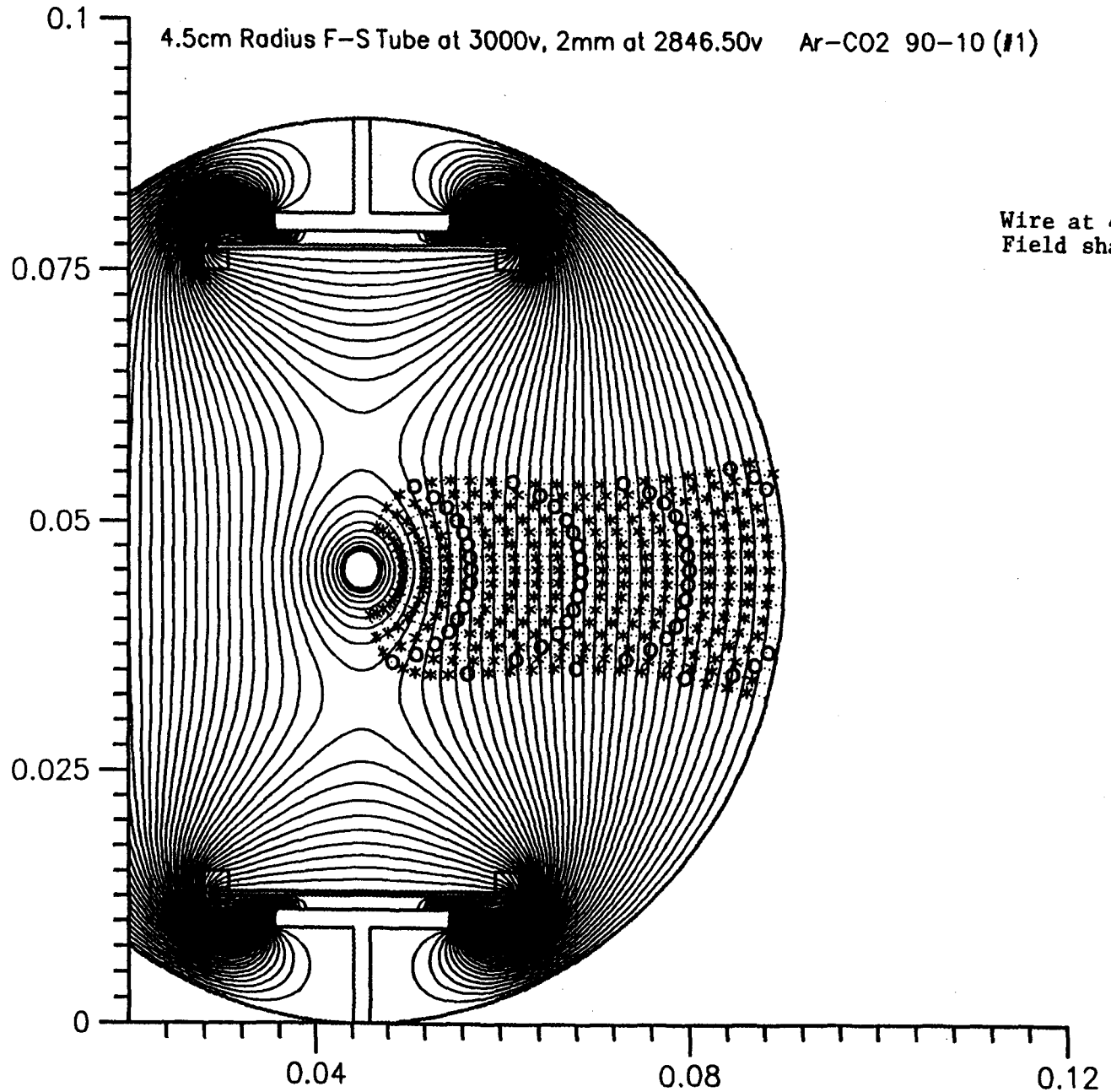

Wire at 4500 volts
Field shaping at 3000 volts

Fig. 20

A plot of drift velocity versus field

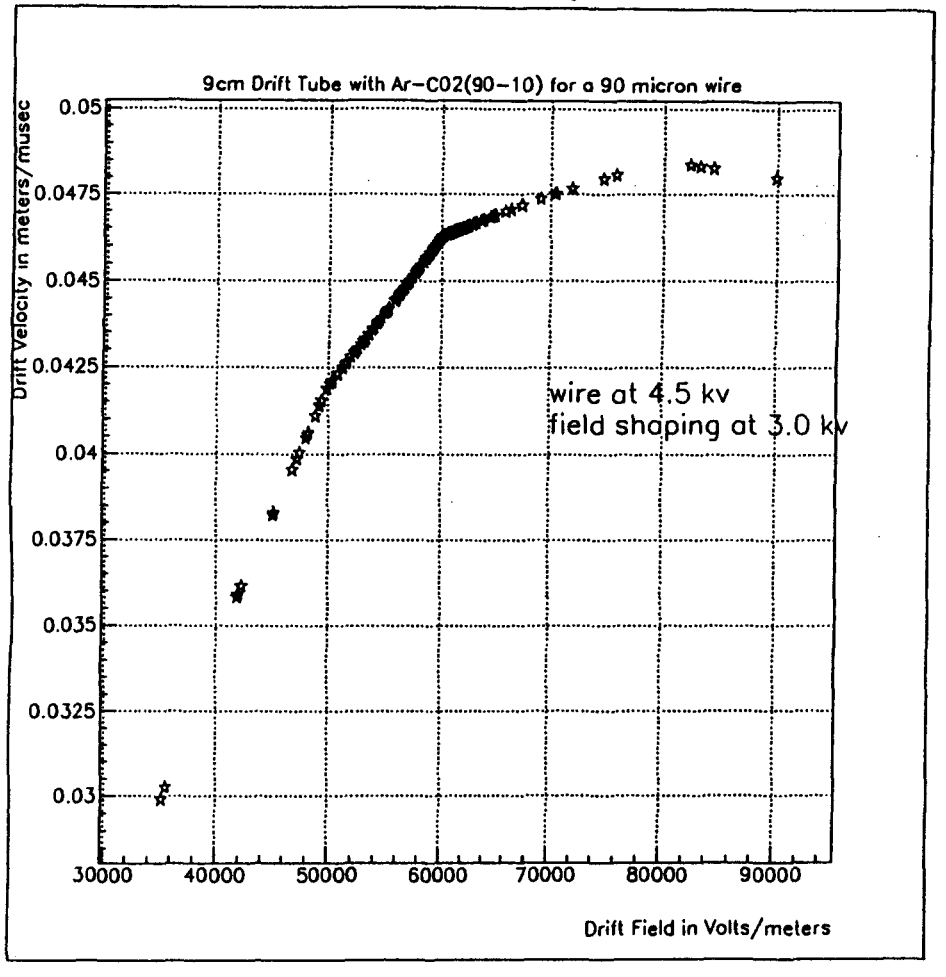

Fig. 21

timer90a4500 = time + 0.99443 - 21.882*(x)

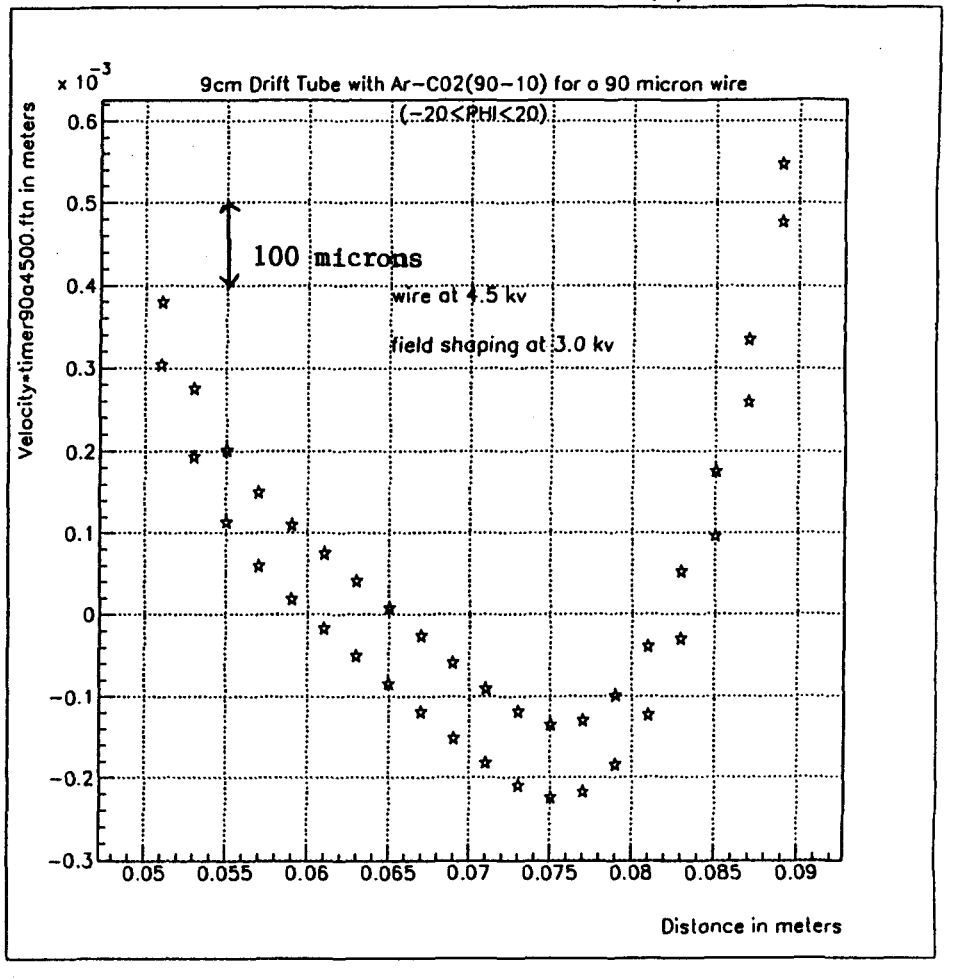

Fig. 22

Wire at 4500 volts
Field shaping at 3000 volts

A linearity plot for upwards displacement of 2mm

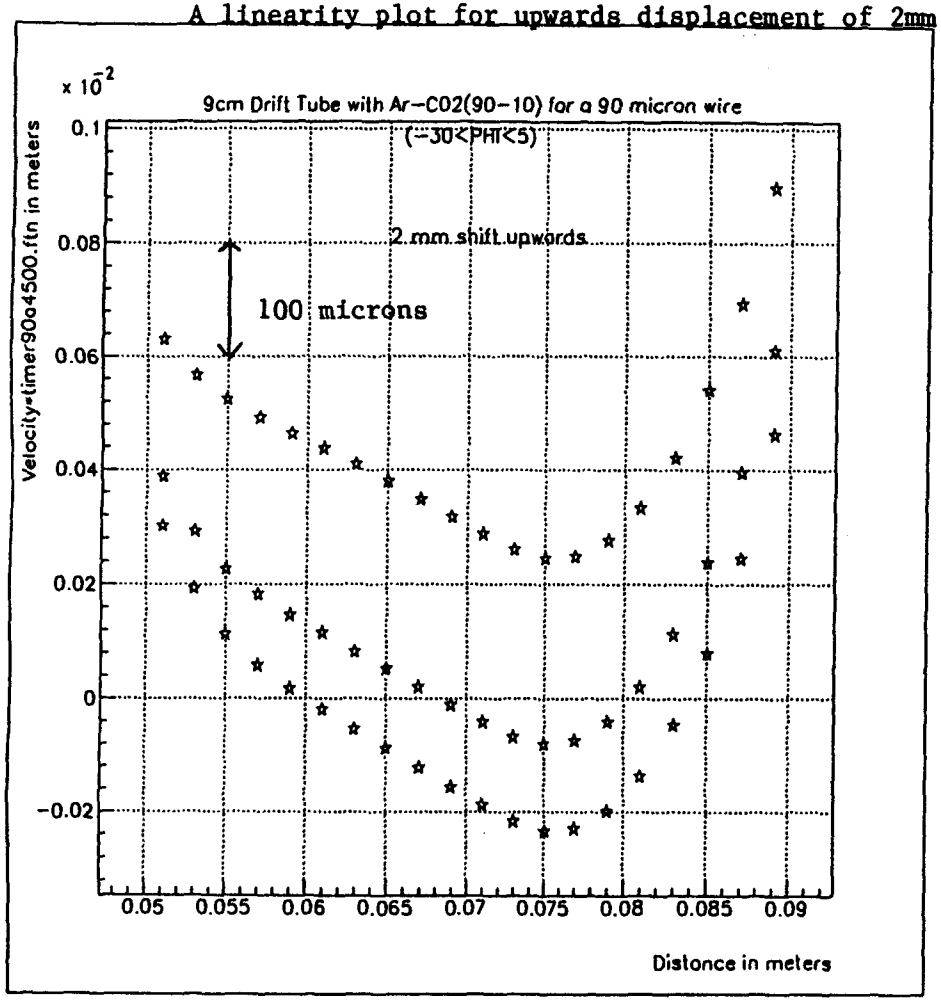

timer90a4500 = time + 0.99443 - 21.882*(x)

Fig. 23

A linearity plot for downward displacement of 2mm

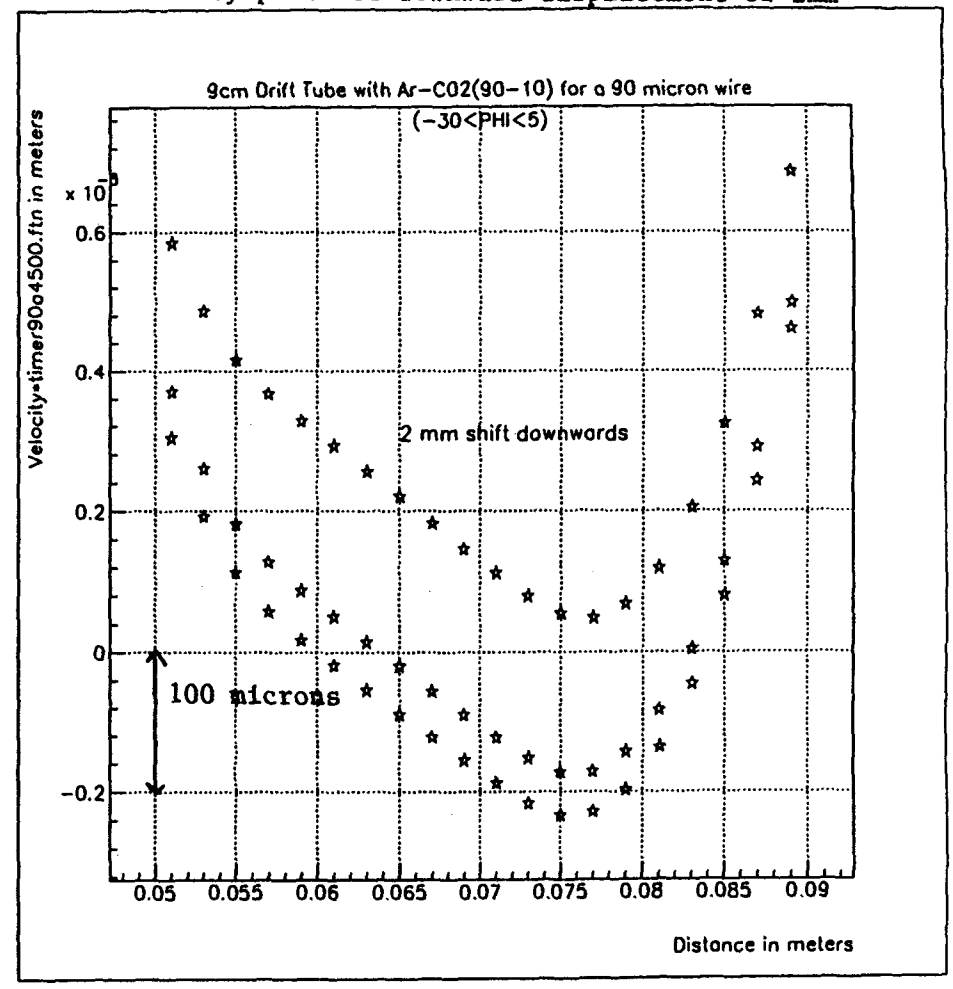

Fig. 24

Wire at 4500 volts
Field shaping at 3000 volts

A linearity plot for left displacement

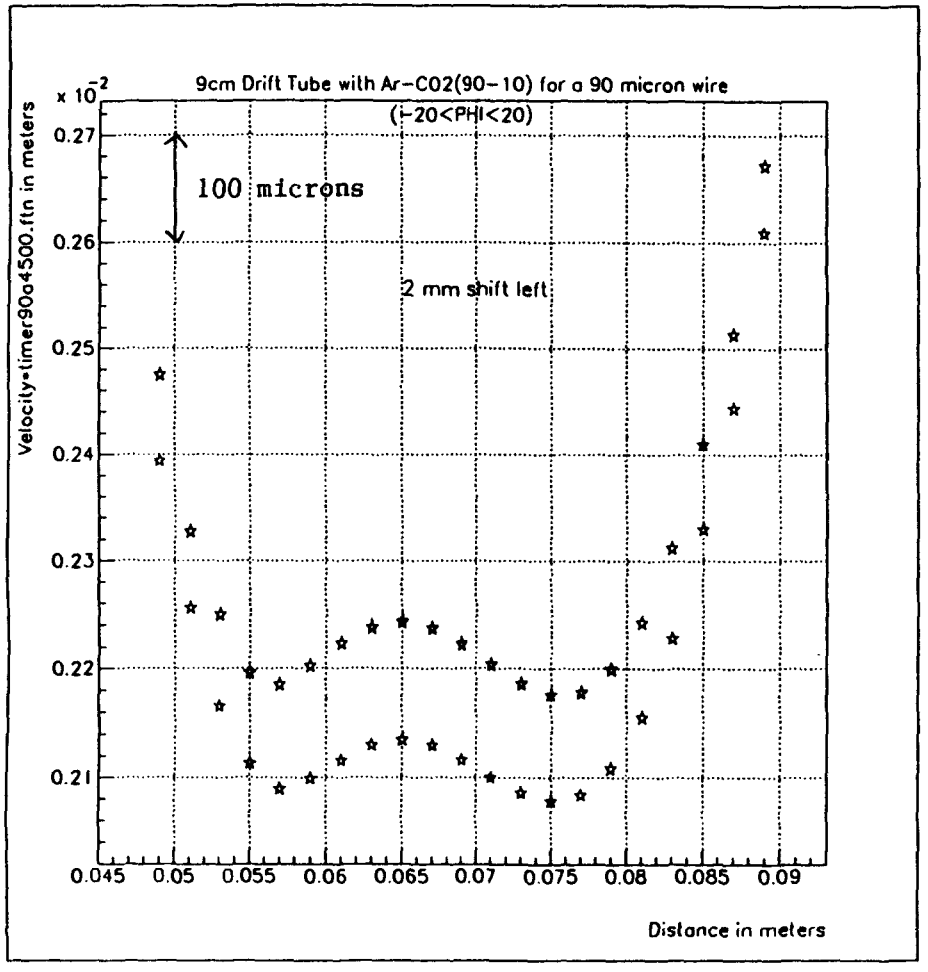

A linearity plot for right displacement

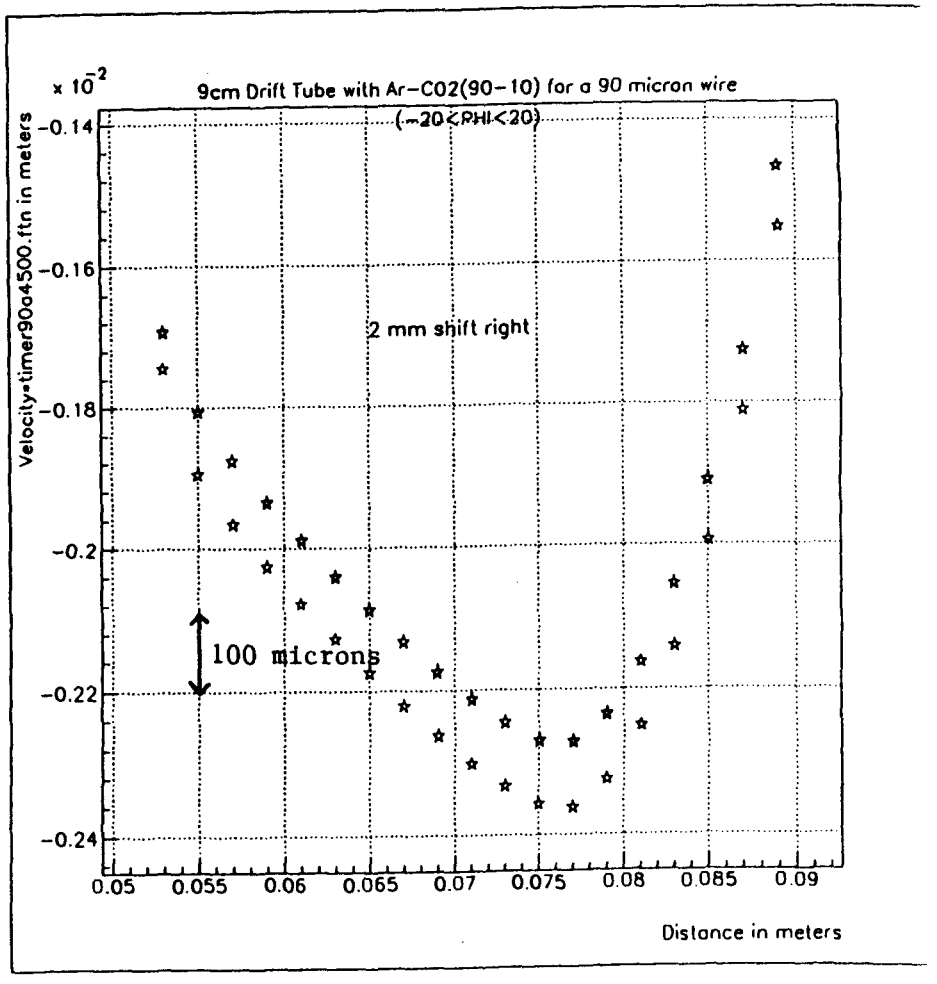

timer90a4500 = time + 0.99443 - 21.882*(x)

Fig. 25

Fig. 26

Fig. 27

A plot of drift velocity versus field

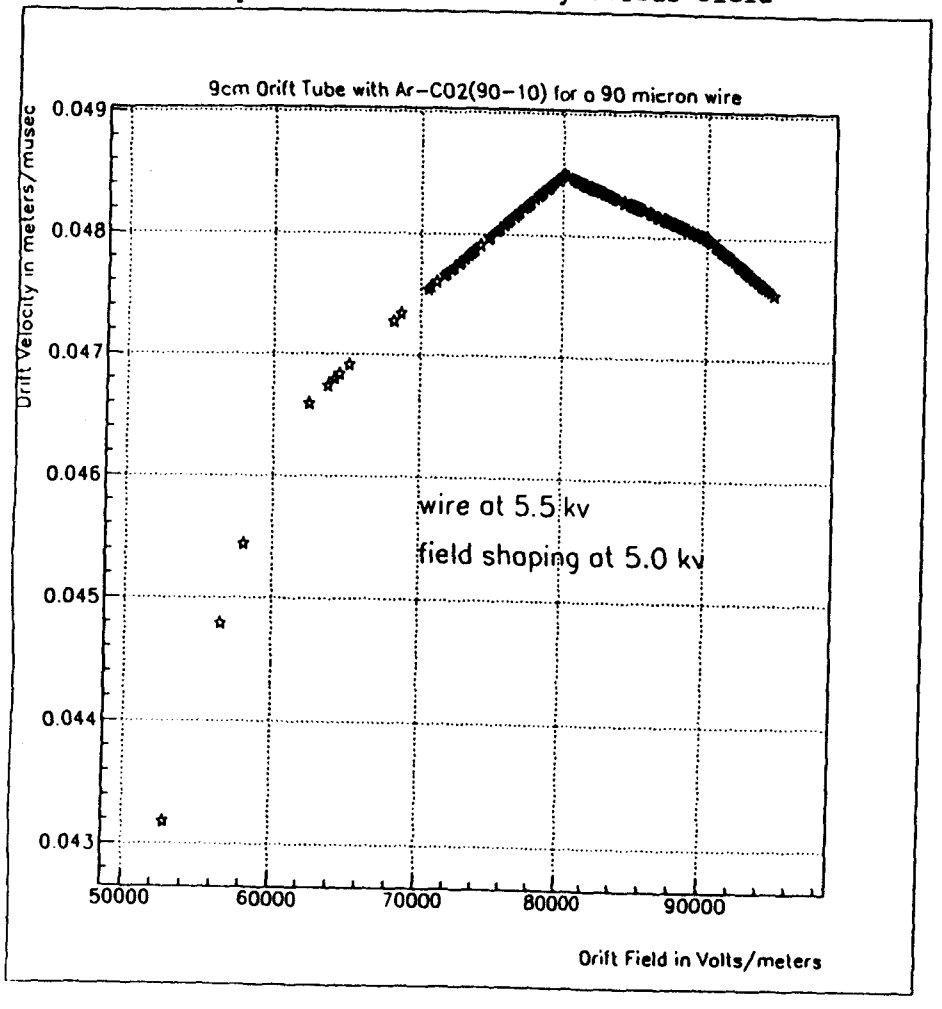

Fig. 28

Linearity plot

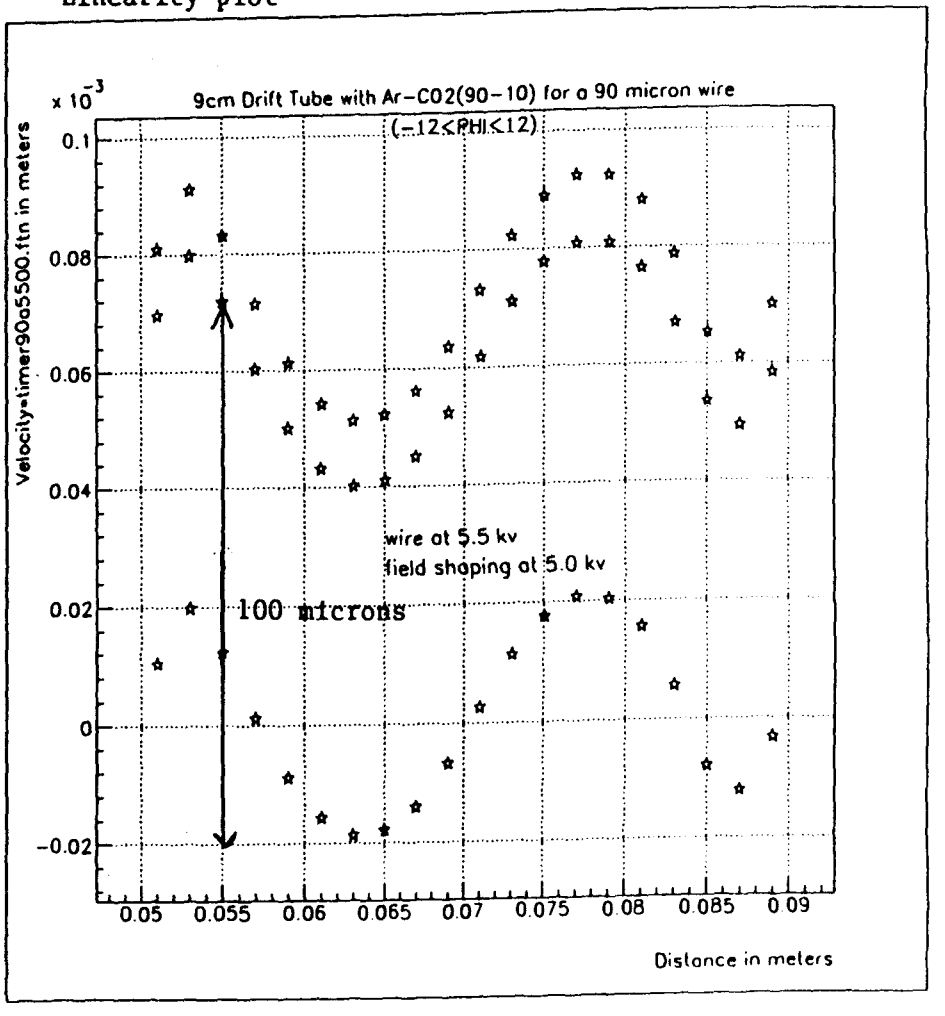

timer90a5500 = time + 0.93140 - 20.781*(x)

Fig. 29

A plot of drift velocity versus field

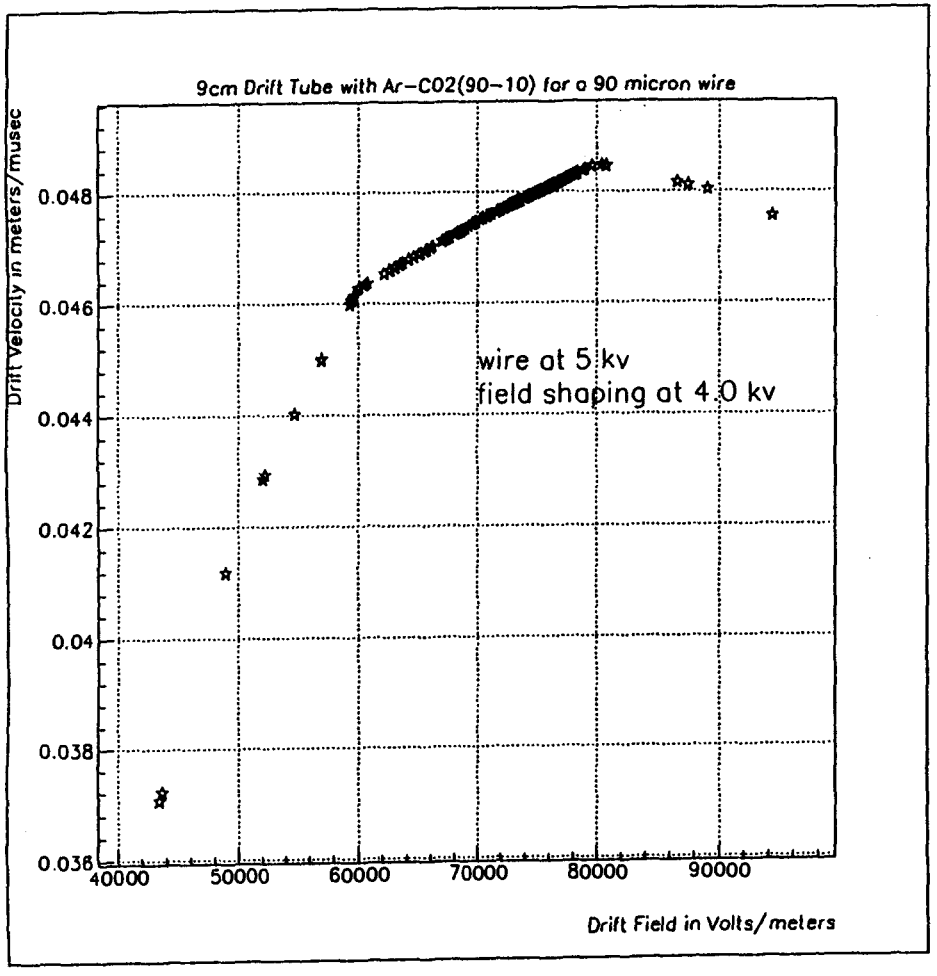

Fig. 30

Linearity plot

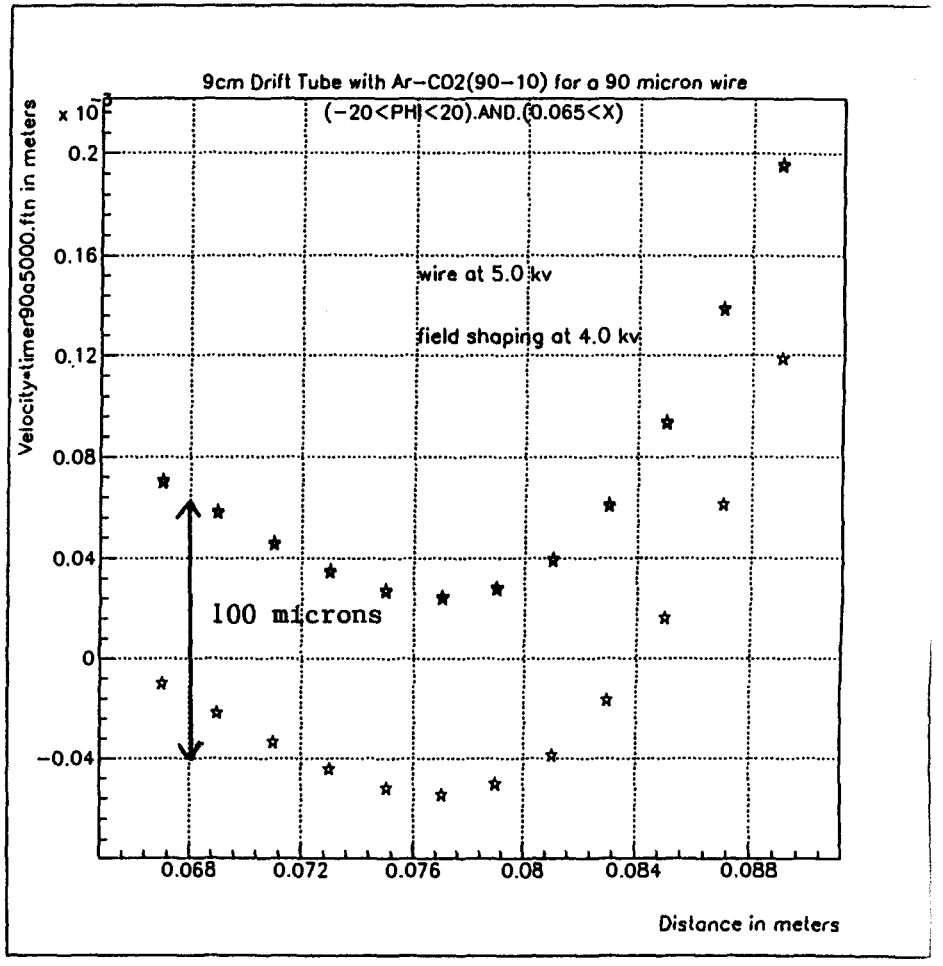

timer90a5000 = time + 0.93945 - 20.917*(x)

A plot of drift velocity versus field

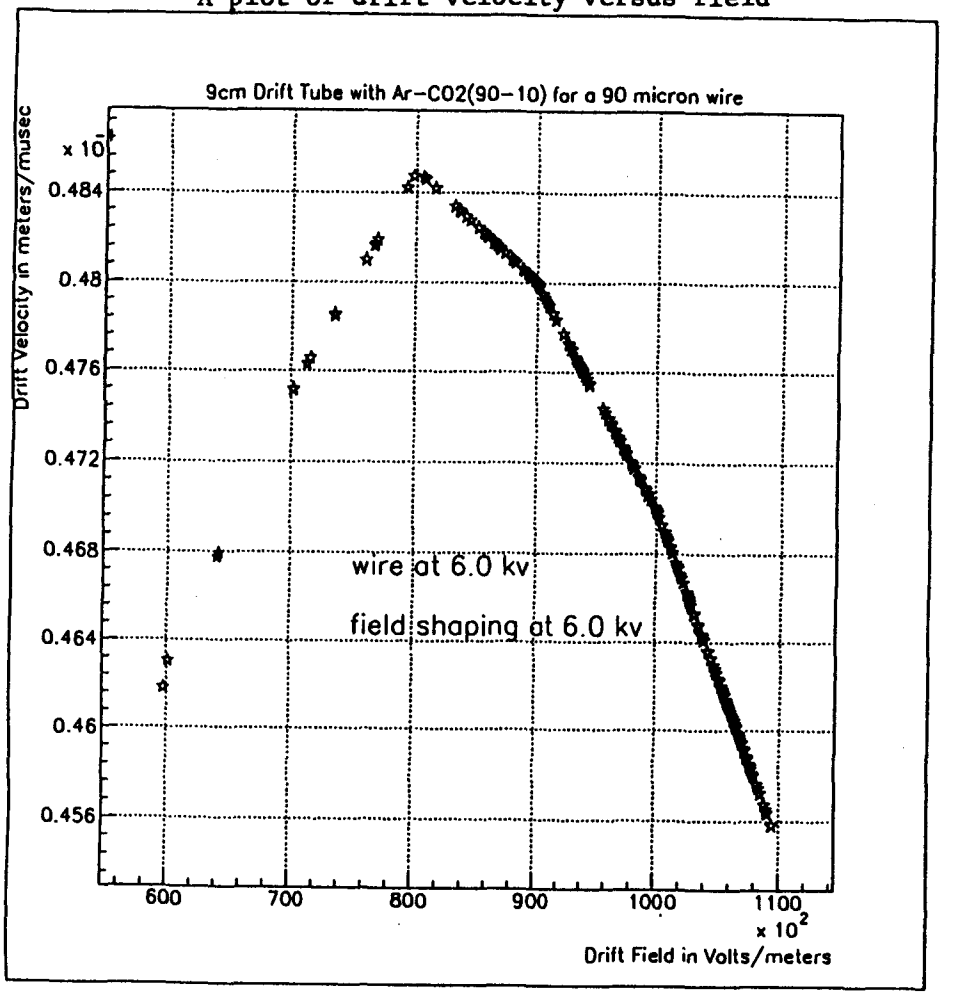

Fig. 31

Linearity plot

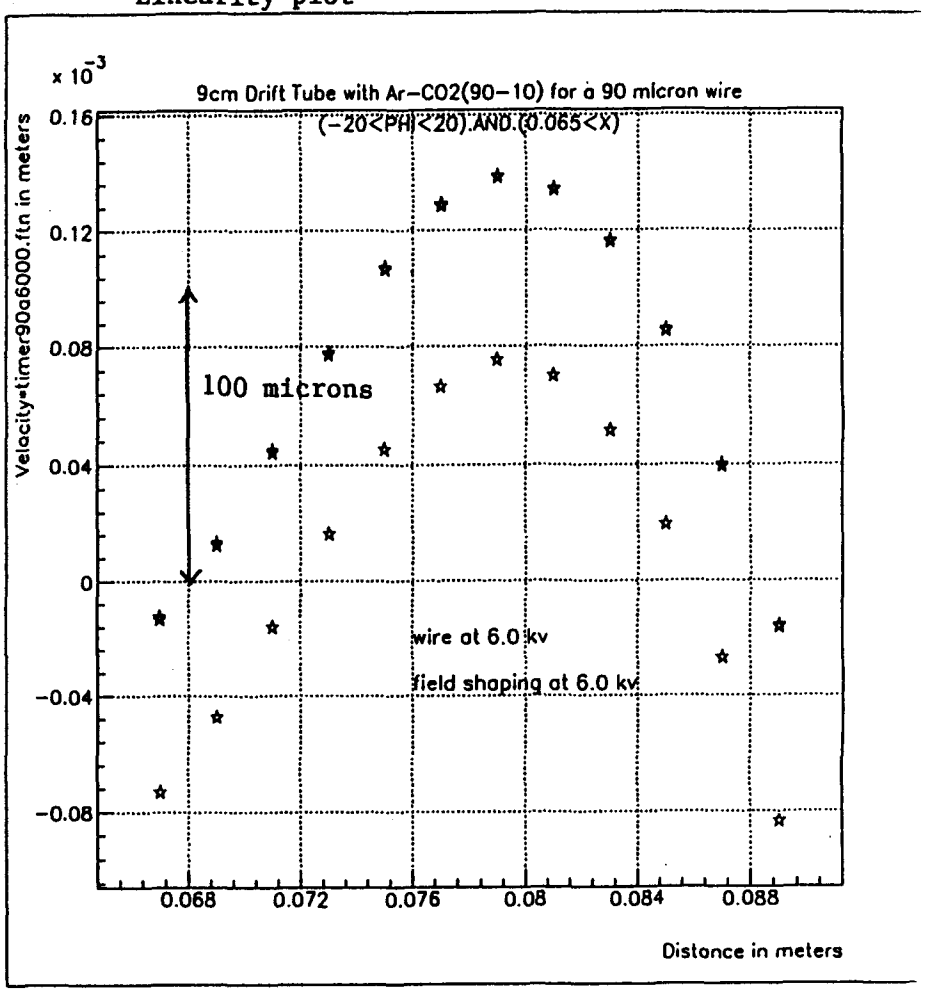

timer90a6000 = time + 0.96237 - 21.357*(x)

Fig. 32

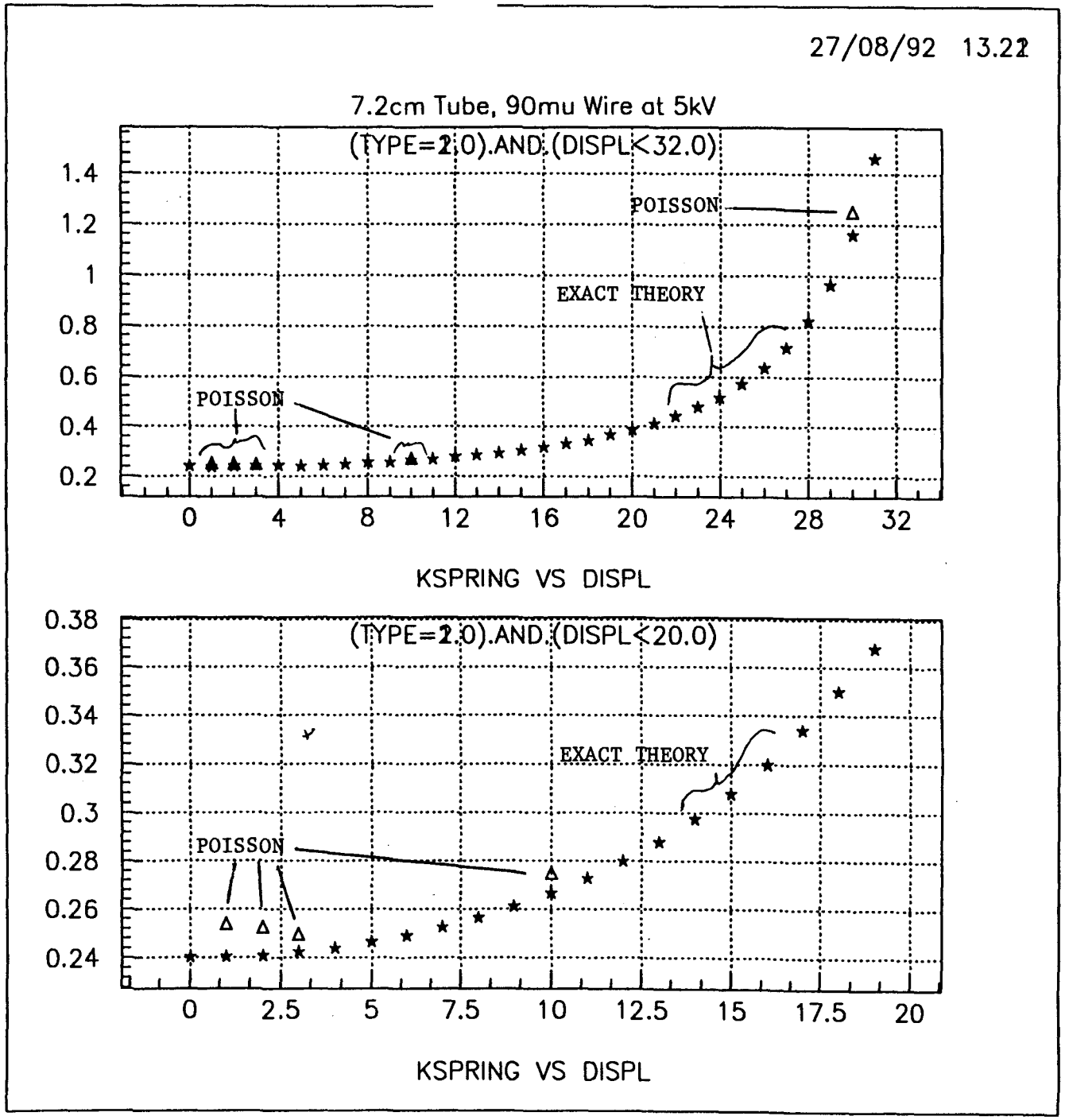
27/08/92 13.22
7.2cm Tube, 90mu Wire at 5kV
(TYPE=2.0).AND.(DISPL<32.0)
POISSON
EXACT THEORY
POISSON
1.4
1.2
1
0.8
0.6
0.4
0.2
0
4
8
12
16
20
24
28
32
KSPRING VS DISPL
(TYPE=2.0).AND.(DISPL<20.0)
EXACT THEORY
POISSON
0.38
0.36
0.34
0.32
0.3
0.28
0.26
0.24
0
2.5
5
7.5
10
12.5
15
17.5
20
KSPRING VS DISPL

Fig. 33